Development of Gerdien condenser for Atmospheric Pressure Plasmas

A dissertation submitted in partial fulfillment
of the requirements for the degree of
PhD in Electronics and Electrical Engineering

The Graduate School of Science and Engineering
Doshisha University

Ma Camille Corrales Lacdan

March 2017

Synopsis

Plasma diagnostics plays an important part in understanding the role of charged particles during plasma processes. However, since common plasma diagnostic techniques are limited to low-pressure case, there is a need for the development of a new diagnostic method specifically for atmospheric pressure plasma characterization. In this study, a diagnostic technique based on the theory of Gerdien condenser method is developed for laboratory-produced atmospheric pressure plasma. The Gerdien condenser, which is a classical instrument employed in atmospheric science, is capable in measuring the ion mobility and density from an obtained current-voltage (*I-V*) characteristics.

In Chapter 2, two atmospheric plasma sources are made operational using a 13.56 MHz RF power supply. The developed atmospheric plasma sources exhibit a dense and a dilute plasma plume due to the difference in device configurations. The plasma plume produced by the compact atmospheric-pressure plasma devices are qualitatively examined using common diagnostic technique, specifically using optical emission spectroscopy and plasma glow image analysis. The length of the plasma plume produced by the needle-shaped electrode configuration is observed to be directly dependent to the input parameter up to a certain value where saturation of plasma plume length is attained. On the other hand, the plasma plume produced by the capacitively-coupled configuration is very dilute and possesses filamentary structures. The effect of input parameters such as gas flow rate and input power is unobservable

if only Ar gas is introduced into the system. The employment of N_2 swirl gas into the dilute plasma stabilizes the plasma flow out of the capacitively-coupled device yielding a more homogeneous and stable plasma plume. Visible range optical emission spectrum show increase in excited nitrogen species while Ar excited species decreases against an increased flow rate of N_2 swirl gas.

The principle of operation and data analysis of the Gerdien condenser method is presented in Chapter 3. In Chapter 4, the applicability of a miniaturized pointed inner electrode Gerdien condenser as a diagnostic tool for atmospheric-pressure plasma is examined. Atmospheric pressure plasmas are generated at 25 W by supplying Ar as main gas and N_2 as swirl gas both with the flow rates of 3 liters per minute using the capacitively coupled configuration. The ion mobilities calculated from the *I-V* characteristics are identified to be those of O^+, O_2^+, Ar^+, and N_2^+. The ion densities for varying pen-to-inlet distance are determined to be in the range from 8 x 10^5 to 2 x $10^7 cm^{-3}$.

An improved version of the miniaturized Gerdien condenser is designed, tested and developed as discussed in Chapter 5. The previous Gerdien condenser design is capable of determining the ion density and mobility, thus ion species composition of the plasma. However, further improvements are done in order to minimize the effect of noise to the signal. The new device has a 1.0 cm diameter, 6.0 cm long cylindrical current collector electrode mounted on a bias electrode of 1.7 cm inner diameter. The new instrument also employs an aluminum-made rectangular box which acts as the electrostatic shield from unwanted noise. It is concluded the shielded Gerdien condenser yielded improved data measured in terms of the reduction of noise contribution to the signal. Two atmospheric plasma sources producing dense and dilute plasma are studied using the new version of the Gerdien condenser. Same ion

mobilities are detected for both atmospheric pressure plasma sources. O^-, O^+, O_2^-, O_2^+, Ar^+ and N_2^+ are assumed to be present in the plasma through the analyzed *I-V* characteristics. The density of the plasma produced by the needle-shaped electrode configuration yielded more than twice of that detected from the capacitively-coupled setup.

The effect of the flow rate of the fan attached at the end of the condenser is investigated by setting the fan flow from 1.9 to 7.5 x 10^2 cm^3s^{-1}. The increase in air flow rate on the Gerdien condenser resulted in a decrease in ion density due to possible enhancement of neutral-ion recombination.

Effects due to kind of materials used for the collector electrode of a Gerdien condenser upon the current-voltage characteristics are also presented in Chapter 6. Aluminum, copper and nickel electrodes are initially polished and cleaned and the *I-V* characteristics are recorded with 15-minutes interval under exposure to ambient air. Results showed that the zero-crossing voltage in the *I-V* curve shifted toward negative electrical potential, while the saturation current decreased in accordance with the passage of time. The electrode surfaces showed clear change in the color after operation. Ion mobilities and ion species concentrations are determined from the measured *I-V* characteristics and they indicate sizable difference by the electrode aging effect. The aluminum electrode showed stable positive and negative saturation currents within 180 minutes, however the saturation current decreased down to 50% of the initial value.

The edge effect to the current-voltage characteristics of the Gerdien condenser is studied through simulation in order to explain the signal current reduction at higher voltage in the *I-V* characteristics. Although results show that the predominant factor on the decrease in measured current is not the edge effect, further investigation is still

needed to confirm the air velocity inside the conduit as well as the possible effect of space charge and neutral-ion recombination contribution to the measurement.

Acknowledgements

I would like to give my sincerest gratitude and appreciation to the following people who have directly and indirectly contributed to this dissertation:

Professor Motoi Wada, for his guidance, knowledge, and encouragement throughout my stay in Doshisha University. He has given me a lot of opportunities so that I can improve my skills and character as a researcher. I am greatly honored to be one of his advisee.

To **Yoshida Scholarship Foundation**, for their generous provision of my tuition and stipend during my three years as a PhD student in Japan. The learning excursion trips they held every year are one of the things I look forward to every summer. I would also like to thank the **Harris Science School Foundation Grant of Doshisha University** which provided me additional support during my first year as a PhD student. This work is also supported by **JSPS KAKENHI Grant Number 15K13611**.

To the faculty and members of **Plasma Physics Laboratory** in Doshisha University, thank you for welcoming me and making my stay enjoyable. Special thanks to **Kota Ogino**, who has always been there in helping me make the Gerdien condenser work and teaching me valuable insights especially in electronics.

To my friends, **Bei, Cafa, Arn and Kim**, for all the helpful insights, late-nights, dinners, *gala*'s and *kape-kape*'s. To all the members of **Assembly Kyoto Church**, for all the prayers and support, for being my second family here in Japan.

To my family, **Papa, Mama, Achi Trish and Kuya Landz, Bro Carlz, Lele and Audreypot**, for all the love and encouragement, for being extremely supportive, for believing in me more than what I am capable of, you are my inspiration!

Above all--- to God be all the glory, honor and praise!

ありがとうございました。 *Thank you very much.* Maraming salamat. *Agyamanak.*

Table of Contents

List of Tables

List of Figures

Chapter 1
Introduction

1.1 Overview

This dissertation presents a new diagnostic technique for laboratory-produced atmospheric pressure plasma characterization based on the theory of Gerdien condenser method. The Gerdien condenser is a classical instrument employed in atmospheric science which can measure the ion mobility and density from an obtained current-voltage characteristics. In order to understand the principle of operation of the Gerdien condenser, the traditional usage of the device is explored and discussed in this research. The instrumentation as well as the theory and the actual experimental behavior of the current-voltage characteristics of the Gerdien condenser are studied.

The plasma that are investigated in this research are produced using atmospheric ion sources that are made operational by a 13.56 MHz RF power supply. The plasma plume produced by the ion sources are examined using common characterization techniques, specifically using optical emission spectroscopy and plasma glow image analysis. The effect of the input parameters such as input forward power and gas flow rates to the produced plasma plume are also studied.

The Gerdien condenser is miniaturized to match the dimensions of plasma produced by the atmospheric pressure ion sources. The designed Gerdien condenser is

shown to be capable of identifying ion species and their corresponding densities of the laboratory-produced atmospheric pressure plasmas. Improvements on the design as well as in data acquisition are also presented.

Although the Gerdien condenser has been utilized for many years in investigating the characteristics of ions in different layers of the atmosphere, there are a lot of studies that are yet to be explored especially with the individual components of the Gerdien condenser. Thus, this research also attempts to discuss the effect of the individual components of the miniaturized Gerdien condenser to the acquired plasma parameters.

1.2 Objectives and Motivations

The study of charged particles present in the plasma is of great interest especially for plasma applications. Plasma diagnostics can be employed in order to comprehensively understand the role of plasma species and how the plasma processes can be optimized. However, the available plasma diagnostics for atmospheric pressure plasmas are limited due to the fact that the common diagnostic techniques are developed for low-pressure condition. Hence, the main objective of this research is to introduce a new diagnostic technique that is particularly suitable for atmospheric pressure plasma characterization.

The Gerdien condenser has several advantages over common plasma diagnostic techniques; the technique is non-invasive yet the plasma species present can be determined simultaneously with their corresponding densities. In addition, the theory used in developing the Gerdien condenser method is established for atmospheric condition. Also, the plasma species present in remote atmospheric pressure plasma applications can be well characterized since the Gerdien condenser can measure even

for low ion density conditions. Therefore, this research aims to establish the instrumentation, method and as well as analysis of Gerdien condenser technique for laboratory-produced atmospheric pressure plasma applications.

1.3 Organization

Chapter 2 provides the fundamental theory related to atmospheric pressure plasma sources as well as experimental results on plasma production using two ion sources with different device configurations. Qualitative plasma plume characterization using emission spectroscopy and plasma glow image analysis are also added in Chapter 2. Chapter 3 presents the fundamentals of atmospheric ion measurement, Gerdien condenser principle and instrumentation, and current-voltage characteristics analysis of a Gerdien condenser. Chapter 4 discusses the miniaturization of Gerdien condenser for laboratory-produced atmospheric pressure plasma usage with the instrument patterned to the one utilized in atmospheric science. Chapter 5 presents the improvement on the miniaturized Gerdien condenser design as well as experimental results on the utilization of Gerdien condenser on dilute and dense atmospheric pressure plasmas. Chapter 6 discusses the effect of the individual components of the Gerdien condenser with the obtained plasma parameter. Finally, Chapter 7 summarizes the research findings of this dissertation and recommends related further research.

Chapter 2
Atmospheric pressure plasma

2.1 Definition of plasma

Plasma, often referred to as the fourth state of matter constitutes more than 99% of the matter in the universe. The stars are made of plasma and much of the space between the stars is occupied by plasma. The most common definition of plasma is that it is partially or fully ionized gas. Hence, it consists of positive and negative ions and electrons, as well as neutral species which are in fundamental and excited states. From a macroscopic point of view, plasma is electrically neutral, that is, the negatively charged particle density is equal to the positively charged particle density to within a fraction of a percent. However, it contains free charge carriers and is electrically conductive at low frequencies but at sufficiently high frequencies its response is more characteristics of a dielectric medium (Tendero *et al.* 2006).

Similar to the plasma in the space, artificially produced plasmas on earth can be classified as either hot dense plasmas or cold dilute plasmas. In the former class are the fully ionized media encountered in research in controlled thermonuclear fusion for power generation, where the challenge is to confine a very hot and dense plasma for a time long enough so that light nuclei will fuse, liberating huge amounts of energy (Chabert *et al.* 2011). On the other hand, the cold dilute plasmas are weakly ionized.

Also called low-temperature plasmas, weakly ionized plasmas includes those used in various industrial applications from welding to semiconductor processing. Low-temperature plasmas are created by applying electrical discharges to a gas in order to reorganize the electronic structure of the species (atoms, molecules) and to produce excited species and ions (Conrads *et al.* 2000). The electrical discharges utilize sources ranging from DC to microwave frequencies. The gas pressure is typically between a fraction of one pascal to a few times atmospheric pressure (10^5 Pa).

In general, plasmas can be categorized according to the temperature of its species (electron, ion, neutral species); plasmas which are in thermal equilibrium and which are not in thermal equilibrium. High temperatures are required to form equilibrium plasmas, typically ranging from 4000 K to 20000 K. Often, the term local thermal equilibrium (LTE) is used which implies that the temperatures of all plasma species are the same in localized areas in the plasma. On the other hand, plasmas which contain species possessing different temperatures are called non-local thermal equilibrium (non-LTE). More precisely, the electrons have higher temperatures than the heavy particles such as ions, atoms, and molecules (Bogaerts *et al.* 2002). The electron density in an LTE plasma is in the range of 10^{21} to 10^{26} m^{-3}, whereas the electron density in non-LTE plasma is lower than 10^{19} m^{-3} (Merche *et al.* 2012).

2.2 Introduction to atmospheric pressure plasma

Atmospheric pressure plasma (APP) refers to a plasma excited at ambient pressure. When the pressure becomes higher, species collisions also build up. This in turn induces both plasma chemistry through inelastic collision, and heavy particles heating by elastic collisions. Compared to low pressure plasma, the difference between

electron temperature and heavy particle temperature for atmospheric pressure case is reduced. The density of the input power influences a lot the plasma state whether it will reach LTE or not. Generally, a high power density induces LTE plasmas such as arc plasmas whereas non-LTE plasmas are produced either by a low density input power or a pulsed power supply (Tendero *et al.* 2006).

By using noble gases such as He and Ar, or N_2 or air, it is possible to obtain glow discharge at atmospheric pressure. However, the glow discharge produced at atmospheric pressure is usually inhomogeneous, such as in the case of low pressure glow discharge (Kong *et al.* 2009). The inhomogeneous atmospheric plasma usually possesses filamentary structures which can be disadvantageous for atmospheric pressure plasma processes. Because of this, the application of atmospheric-pressure plasmas can be limited. On the other hand, the produced localization of atmospheric pressure plasmas can be advantageous for exposing plasma into hard-to-reach regions such as porous and hollow surfaces.

Atmospheric pressure plasmas have been gaining attention over the years in research mainly due to their ease of use for not requiring vacuum equipment. The advantage reduces the cost for developing atmospheric pressure plasma device and enlarges the dimension of materials to be treated by plasma. Nowadays, atmospheric plasmas are being utilized in various areas of research such as in biotechnology, medical applications, remediation of pollutants, nanotechnology and surface processing. Cold atmospheric pressure plasma sources that are utilized for biotechnology and medical applications are recently miniaturized such that they can be handheld and portable. Meanwhile, atmospheric plasma sources for surface processing such as those for industrial applications are arranged in arrays for more uniform plasma applications.

2.3 Atmospheric pressure plasma sources

2.3.1 Overview of various atmospheric plasma sources

Atmospheric pressure plasma sources can be classified regarding their excitation mode. The excitation frequency for plasma production plays an important role since it influences the behavior of the electrons and ions. Figure 2.1 shows an example of the range of electron plasma frequency (*fpe*) and ion plasma frequency (*fpi*) in cold plasmas such as in glow discharges as discussed by Tendero *et al.* (2006). Equations (2.1) and (2.2) show the equation of electron and ion plasma frequency, respectively.

$$\omega_{p_e} = \left(\frac{ne^2}{\varepsilon_0 m_e}\right)^{1/2} \tag{2.1}$$

$$\omega_{p_i} = \left(\frac{ne^2}{\varepsilon_0 m_i}\right)^{1/2} \tag{2.2}$$

where, n corresponds to the density of negative or positive charges which are almost equal, m_e and m_i corresponds to the electronic and ionic masses, respectively, and ε_0 is the permittivity in vacuum, with $\omega_{p_e} = 2\pi fpe$ and $\omega_{p_i} = 2\pi fpi$.

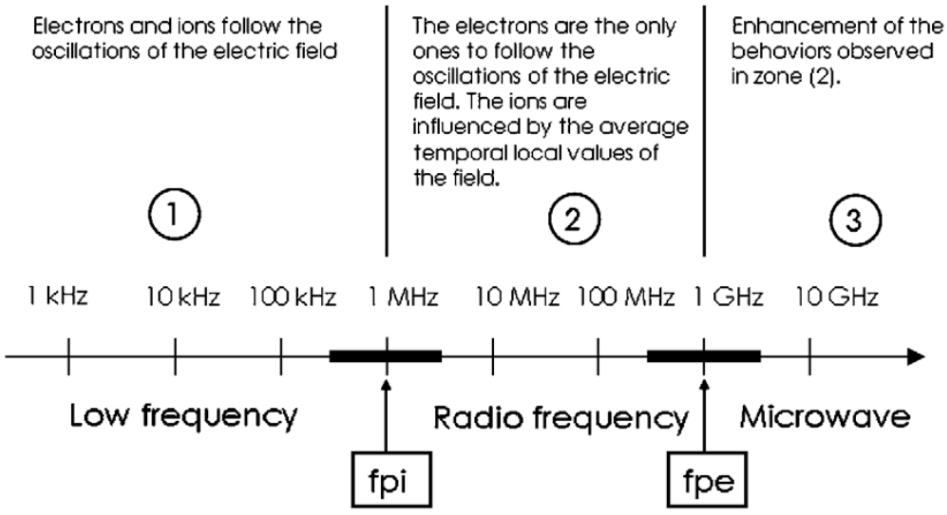

Figure 2.1 Electrons and ions frequencies in cold plasmas (Tendero *et al.* 2006)

Atmospheric pressure plasma sources can also be classified according to their device configuration. Some examples are dielectric barrier discharge, microwave-induced plasma, and RF discharges.

Dielectric barrier discharge (DBD) devices consist of two plane-parallel metal electrodes, wherein at least one of the electrodes is covered by a dielectric layer. Plasma gas flows in the gap that separates the electrodes which is as small as to a few millimeters wide. The DBD can be produced through sinusoidal or pulsed power source.

Microwave systems consists of a microwave power source which includes the magnetron and circulator to protect the magnetron from reflected power, wave guides and tuning system, ignition system, and gas injections. Microwaves are guided along the power delivery system and transmit energy to the plasma gas electrons. Electrons accelerated in the microwave field collide with heavy particles. Due to the large mass of heavy particles, the collided electrons rebound whereas the heavy particles remain static. The electrons are thus accelerated and the heavy particles are slightly heated. After several elastic collisions, the electrons get enough energy to produce inelastic collisions to excite or even ionize heavy particles. The gas is partially ionized and becomes plasma which supports microwave propagation (Kabouzi *et al.* 2002).

2.3.2 Radio-frequency plasmas

Radio-frequency electromagnetic field can be generated in many ways, for instance by applying an RF voltage across two parallel electrodes or by circulating RF currents in coils or antennas that is either immersed in the plasma or separated from it by a dielectric window. The electromagnetic field then couples to the electrons in the plasma and transfer energy to them to sustain the plasma.

The efficiency with which power is coupled from the power supply into the charged particles and the plasma uniformity both strongly depend on the design of the RF wave excitation structure. The two classical RF systems used in the industry are the capacitively coupled plasmas (CCP) and the inductively coupled plasmas (ICP). The CCP system comprises of two electrodes which is separated by a gap of a few centimeters. RF power is then coupled into the plasma through the electrodes.

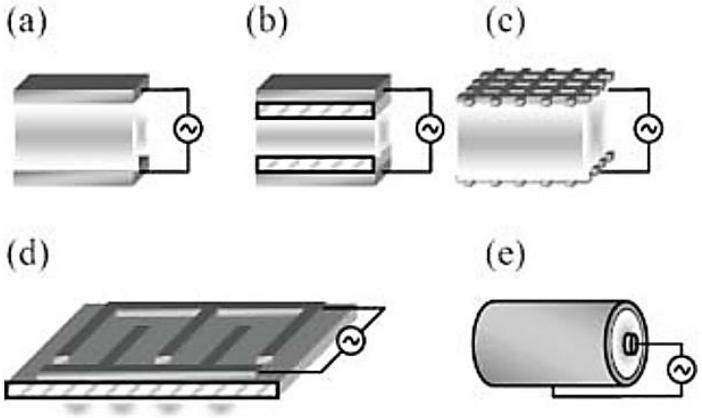

Figure 2.2 Schematics of RF capacitively coupled microplasmas: (a) parallel plate with bare electrodes (b) parallel plate with dielectric-covered electrodes, (c) grid electrodes, (d) comb electrodes, and (e) coaxial jet (Iza *et al.* 2008)

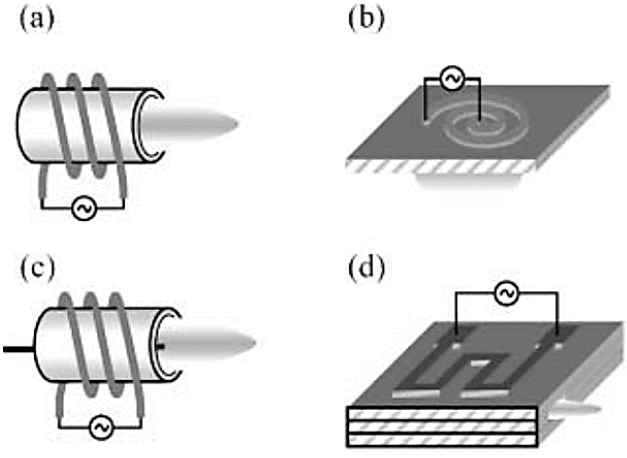

Figure 2.3 Schematics of inductively coupled microplasma sources: (a) coil, (b) planar spiral, (c) coil+filament, and (d) serpentine (Iza *et al.* 2008)

ICP systems uses the RF source to drive a coil which is usually external to the plasma and separated from it by a dielectric window. The RF current flowing in the coil launches an evanescent electromagnetic disturbance that decays over a distance of a few centimeters into the plasma. This induces RF current in the plasma and transfers energy to electrons (Chabert *et al*. 2011).

2.3.2.1 Capacitively-coupled configuration

The 'capacitively coupled' term refers to the way of coupling the input power into the plasma discharge, by means of forming electric field between two electrodes and their sheaths behaves as kind of capacitor. When sustaining a direct current glow discharge, one or both of the electrodes starts to become non-conductive such as when the electrodes become gradually covered with insulating material which reduce the field intensity. Hence, the electrodes will be charged up due to accumulation of positive and negative electrical charges, resulting to the glow discharge to be extinguished. This problem is overcome when an alternating voltage is applied between the two electrodes, so that each electrode will act alternately as a cathode or an anode, and the charge accumulated during one half-cycle will be at least partially neutralized or released by the opposite charge accumulated during the next half-cycle. The excitation frequencies generally used for these alternating voltages are typically in the radiofrequency range of 1 kHz to 10^3 MHz with a most common value of 13.56 MHz. In practice, many radiofrequency glow discharge processes operate at 13.56 MHz, because this is a frequency allotted by international communications authorities at which one can radiate a certain amount of energy without interfering with communications (Bogaerts *et al.* 2002).

Atmospheric pressure plasma devices in capacitively coupled configuration is considered to be practical for atmospheric plasma processes. Besides the simplicity in its electrode configuration, the capacitive discharge can be operated at lower discharge voltage compared to dielectric barrier discharge operated at frequencies of 10 to 100 KHz. The produced plasma plume can be touched by bare hands and can be directed manually by a user to come in contact with delicate objects and materials, including skin and dental gum, without causing any significant heating or painful sensation (Ohtsu *et al.* 2009).

2.4 Atmospheric pressure plasma device schematic

2.4.1 Capacitively-coupled plasma (CCP) device

Figure 2.4 shows the schematic diagram and the actual photo of the atmospheric pressure plasma (APP) source in capacitively-coupled configuration. The APP source consists of a 60 mm long, 50 mm base diameter grounded outer electrode and a 25 mm long hollow cylindrical inner electrode connected to a 13.56 MHz power supply. The gas utilized for plasma production is introduced from the bottom of the outer electrode and is contained by a 57 mm long, 5 mm inner diameter cylindrical quartz tube as shown in Figure 2.4.

The system also has a swirl gas entrance located at the side of the outer electrode. The swirl gas is utilized to stabilize the filamentary structure that is usually produced by APP sources. The RF power supply has a built-in tuning unit to match the impedance between the source and the plasma load. The plasma is generated by inserting a tungsten wire into the discharge tube after the introduction of gas into the system. A high electric field region is created at the tip of the tungsten wire upon transmission of

radiofrequency waves inside the glass tube which then ignites the plasma. The lowest RF input power that can sustain the plasma for the CCP configuration is about 25 W with minimum reflected power of about 10%.

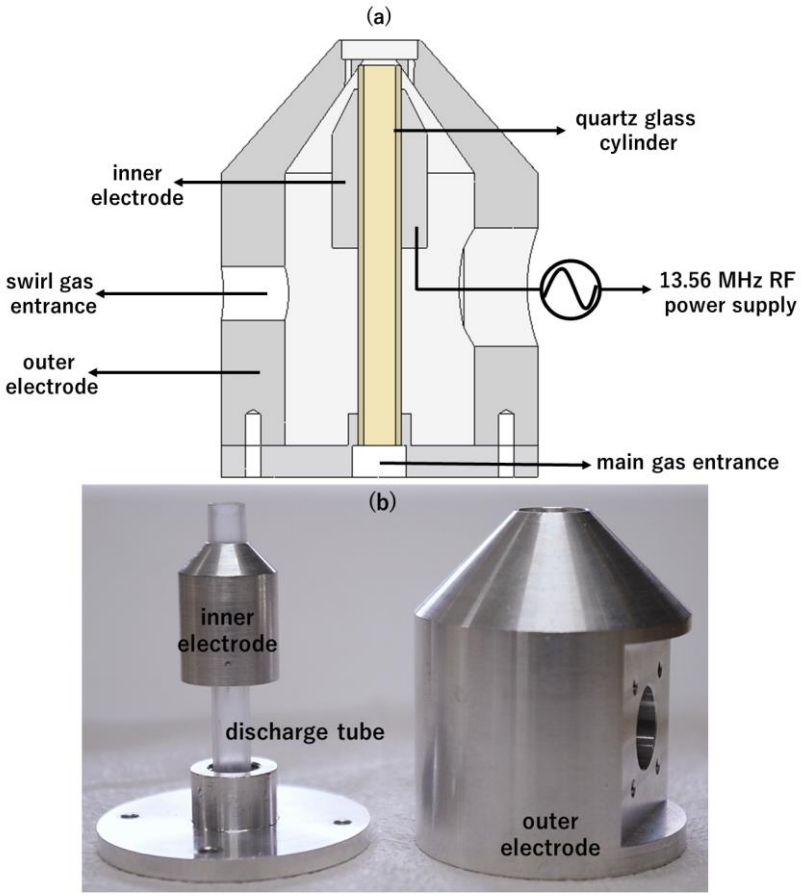

Figure 2.4 (a) Schematic diagram and the (b) actual photo of capacitively-coupled device

2.4.2 Needle-shaped electrode device

Shown in Figure 2.5 is the schematic diagram and actual photo of the APP needle-shaped electrode device. The 41 mm in length outer casing with 15 mm inner diameter acts as the grounded electrode while the 35.5 mm in length and 10 mm in diameter inner copper electrode is connected to a 13.56 MHz power supply. Located on top of the copper electrode is a 1 mm diameter, 13 mm long needle-shaped tungsten rod. The

pointed structure of the tungsten rod is designed to concentrate electric field at the tip. High electric field enough to cause breakdown concentrates at the sharp edge of the tungsten rod thereby sustaining denser plasma compared to the capacitively-coupled configuration. Plasma is sustained even for RF input of as low as 10 W with reflected power less than 5%.

The top part of the outer casing has a tapered nozzle with inner diameter of 2 mm. With this design, the plasma is constricted into a narrower exit producing a pen-like structure as shown in Figure 2.6. Similar to CCP, the plasma is generated by inserting a tungsten wire into the nozzle after introduction of gas into the system. However, since the needle-shaped electrode device does not have a discharge tube which confines the main gas, swirl gas can not be employed into the system.

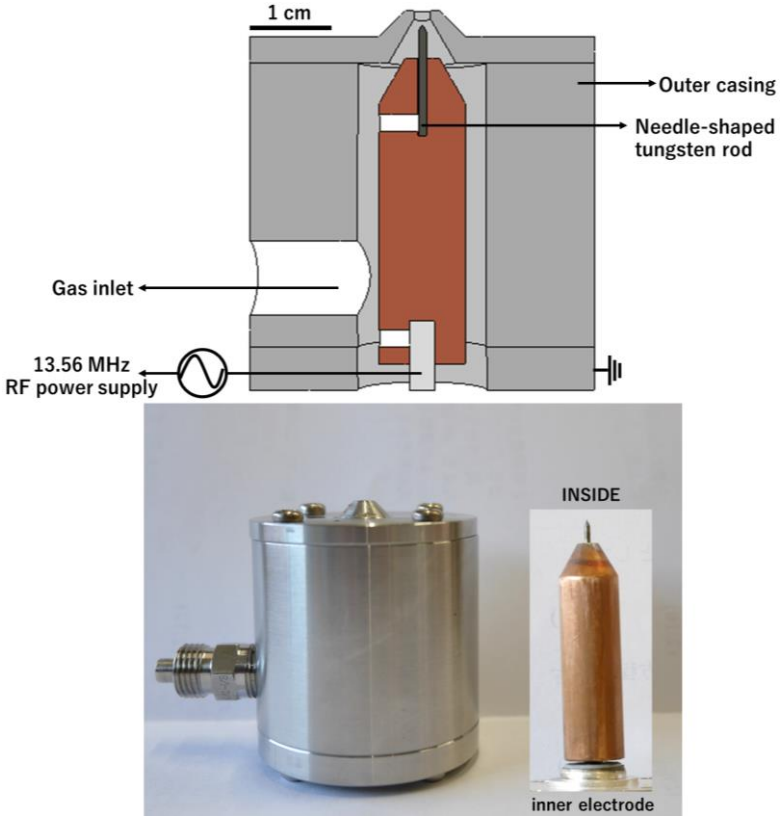

Figure 2.5 Schematic diagram of needle-shaped electrode device

2.5 Plasma diagnostics

Plasma diagnostics plays an essential role in understanding the relationship of plasma parameters to the effectiveness in utilizing plasmas in fields such as biomedicine, nanotechnology and surface processing. There have been a lot of studies on plasma diagnostics for low-pressure plasmas, but a little information is available for atmospheric plasma case. For example, there are several reports on charged particle exposure to inactivate microorganisms; however, the exact role of ions is not yet fully understood (Fridman *et al.* 2007).

It is of great interest to measure the plasma parameters in order to explain the mechanism behind the effectiveness of plasma processing under atmospheric pressure. Interpretations of plasma performance based on plasma diagnostics is also important in improving the plasma process for more complicated applications.

One of the common methods of plasma diagnostics especially for low pressure plasma is the Langmuir probe technique. The simplicity of its construction with ease adaptive to laboratory application and more importantly, its capability for local measurements of plasma parameters have been the primary reasons for the Langmuir probes to be widely used today. The basic assumptions for the Langmuir probe theory are (Schott *et al.* 1968):

(1) The plasma is infinite, homogenous, and quasineutral in the absence of the probe;

(2) The electrons and ions have Maxwellian velocity distributions,

$$f(v) = \left(\frac{m}{2\pi kT}\right)^{1/2} \exp\left(\frac{-mv^2}{2kT}\right) \tag{2.3}$$

with the electron temperature much greater than that of the ion's.

where k is Boltzmann's constant, and the width of the distribution is characterized by the temperature T.

(3) The mean free paths, λ, of the charged species are large compared to any other relevant characteristic lengths *i.e.* collisionless plasma;

$$\lambda = \frac{1}{n_a \sigma} \tag{2.4}$$

where, n_a is the neutral gas atoms density, and assuming that the atoms have cross-sectional area σ.

(4) The charged species do not react with the probe but are absorbed upon contact with it fully contributing to the measured current.

(5) The Debye sheath thickness, a layer of plasma with high density of positive ions, is small compared to the lateral dimensions of the probe. It is common to assume that the sheath around an object will have a thickness of the order of a few Debye lengths, λ_D, where the Debye length is given by the equation:

$$\lambda_D = (\frac{\varepsilon_0 k T_e}{n e^2})^{1/2} \tag{2.5}$$

However, as it is made small for determining local plasma parameters, the Langmuir probe does not yield enough signal amplitude for dilute atmospheric pressure plasma. Langmuir probe technique requires that the ion production rate of plasma discharge to be sufficient so that the current intensity overcomes background noise. There have been attempts (Cada *et al.* 2003; Fanara *et al.* 2001; Porteanu *et al.* 2010; Fridman *et al.* 2007) to use Langmuir probes for atmospheric pressure plasmas, but the theory for atmospheric pressure plasma largely differs from the one for reduced pressure plasma.

2.5.1 Optical emission spectroscopy

Optical emission spectroscopy (OES) is one of the fundamental plasma diagnostic methods. It can be easily utilized for low and atmospheric pressure plasmas and it has no influence on the studied object since it non-invasive, hence it can be utilized for any kinds of plasma. Spectroscopic measurements allow determination of the plasma composition and even their electrical properties such as electron density and energy distribution function can be obtained (Machala *et al.* 2007).

Optical emission spectroscopy technique is easy to implement and measurements are high-speed. The method for OES measurement is passive and based on recording light emitted from the plasma. Through collisions of plasma particles with electrons, plasma particles are excited to higher electronic states. Relaxation of excited particles to lower energy states is the origin of emitted photons of light. Energy of released photon is equal to the difference between excited and lower energy state and corresponding with wavelength of spectral line described by relation:

$$\lambda = \frac{hc}{E_p - E_k} \tag{2.6}$$

where h is Planck's constant, c is the speed of light, E_p and E_k are the upper and lower energy states, respectively. Since the energy of a transition is a characteristic of the particle species, the analysis of the photon energy can reveal the composition of the plasma. It is important to note, that when spectral lines of some particles are not observed by OES, these particles could be still present in discharge plasma but not excited (Kolpaková *et al.* 2011). The composition of the emission spectra gives insight in the in situ plasma chemistry reaction and could be used to account for contribution on plasma application (Mullen *et al.* 1971).

2.6 Plasma plume analysis

2.6.1 Effect of input parameters to APP of needle-shaped electrode device

The plasma plume produced by the needle-shaped electrode device are investigated for varying input forward powers and Ar main gas flow rates. Images of the plasma plume are captured with a *Pentax K7* camera using a fixed shutter speed of 1 sec., aperture of F1/10 and ISO 400 sensitivity. Images are taken for input parameters listed in Table 2.1.

Table 2.1 Input parameter for plasma plume analysis of needle-shaped electrode device

Input forward power (W)	10, 15, 20
Ar gas flow rate (l/min)	1, 3, 5

Figure 2.6 shows the actual images of the plasma plume for varied parameters. After 15 W input forward power, the plume does not significantly increase in length. The longest plasma plume length of about 5.7 mm is attained at 20 W and 5 l/min Ar gas flow rate. For forward powers higher than 25 W, the produced plasma is unstable due to the arcing caused by the tungsten rod needle-shaped electrode to the outer grounded electrode.

The intensity profile of the plasma plume produced by the needle-shaped electrode device for varying gas flow rate and forward power are shown in Figure 2.7 and Figure 2.8, respectively. The obtained plume intensity is directly proportional to the applied forward power and gas flow rate. Hence, it can be deduced qualitatively that higher plasma density can be attained when the input parameter is increased.

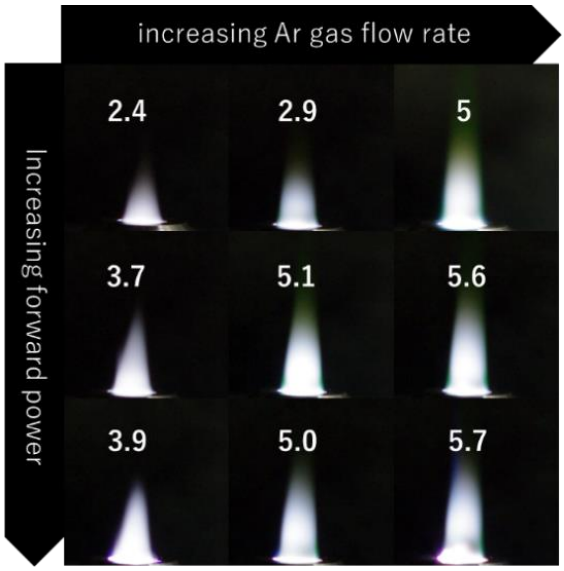

Figure 2.6 Plasma plume produced by the needle-shaped electrode device

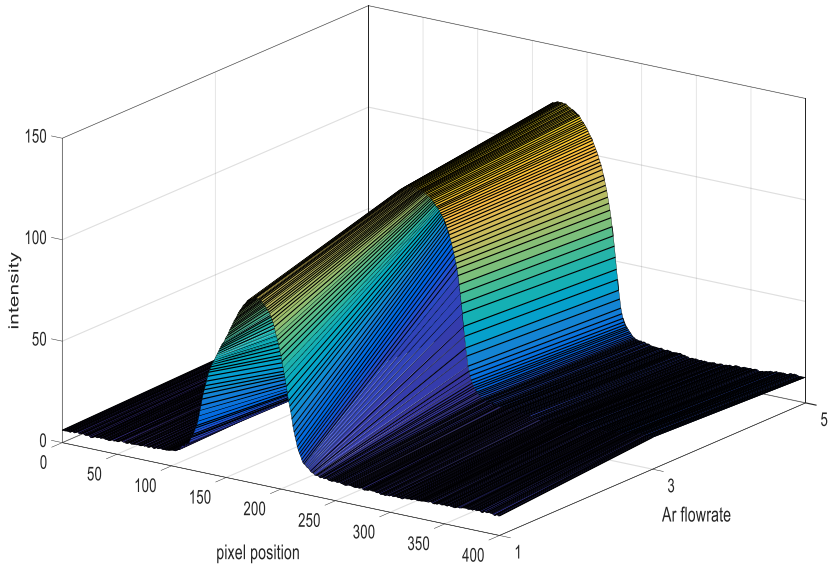

Figure 2.7 Intensity of plasma plume for varying gas flow rate at 15 W input power

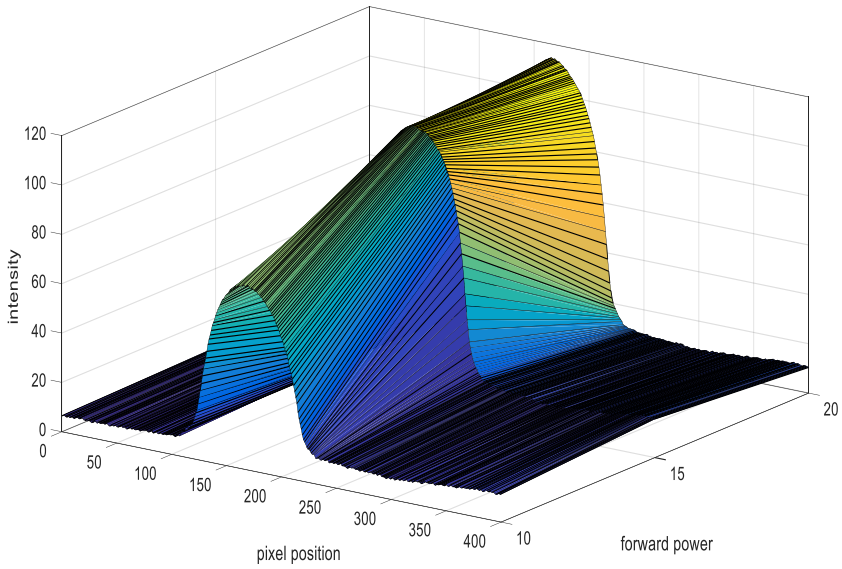

Figure 2.8 Intensity of plasma plume for varying forward power at 3 l/min Ar gas flow rate

In order to investigate the present species in the plasma, the emission spectra of the plasma plume produced by the needle-shaped electrode device is measured using an *USB 4000 Ocean Optics* optical emission spectrometer.

The present species detected by the OES are N_2 I, O I, and Ar I. The presence of oxygen and nitrogen species which are contribution from the ambient air are expected since the needle-shaped electrode device is operated in atmospheric pressure.

2.6.2 Effect of input parameters and swirl gas introduction to CCP device

It has been reported that the employment of swirl gas injection in atmospheric pressure devices stabilize the filamentary structure hence producing a more uniform plume discharge. To understand the effect of swirl gas on atmospheric pressure plasma, the dependence of plume length and plasma species to swirl gas flow rate are investigated. In this study, the APP source in capacitively-coupled configuration shown

in Figure 2.4 is utilized. Ar with gas flow rate of 5 l/min is utilized as the plasma gas while N_2 of varied flow rate as shown in Table 2.2 is utilized as the swirl gas. Here, it should be noted that the swirl gas does not mix with the main gas when introduced into the system. Instead, the swirl gas exits around the produced plasma plume. The main gas which is used for plasma production is confined using a quartz cylinder glass tube as shown in Figure 2.10.

Images of the plasma plume for different input parameters were captured using *Pentax K7* camera with fixed shutter speed of 1.3 sec, aperture of F5.6 and ISO 800 sensitivity. The emission spectra of plasma produced at various input parameters are recorded using a USB 4000 optical emission spectrometer from *Ocean Optics*.

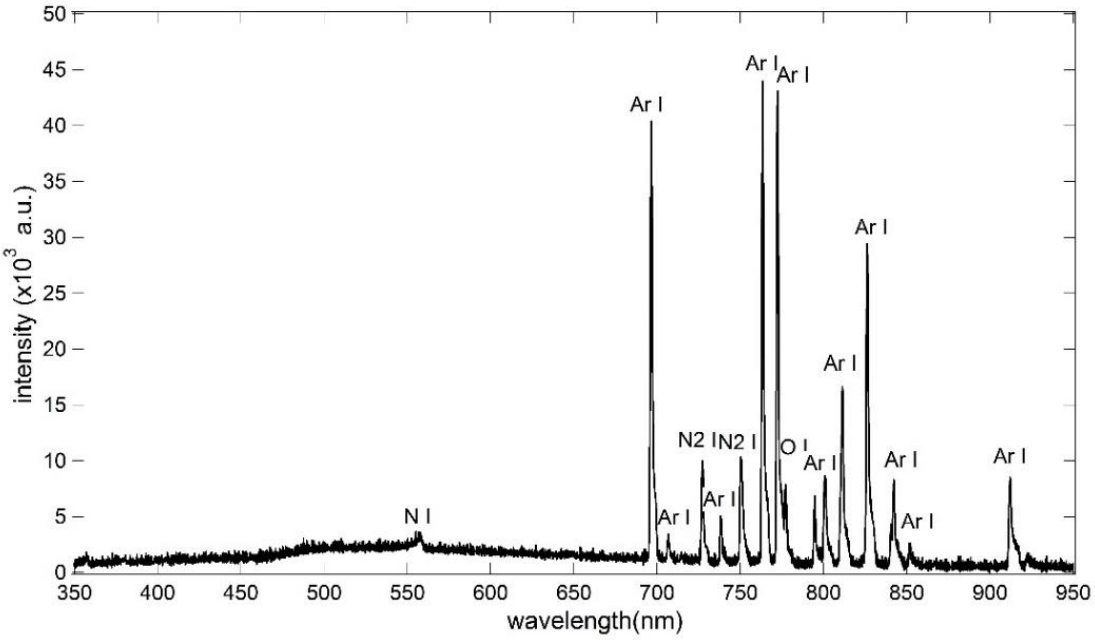

Figure 2.9 Typical emission spectrograph of the plasma produced by needle-shaped electrode device

Table 2.2 Input parameter utilized for capacitively-coupled device setup

Input forward power (W)	25, 30, 35, 40
N_2 swirl gas flow rate (l/min)	0, 1, 3, 5
Ar main gas flow rate (l/min)	5

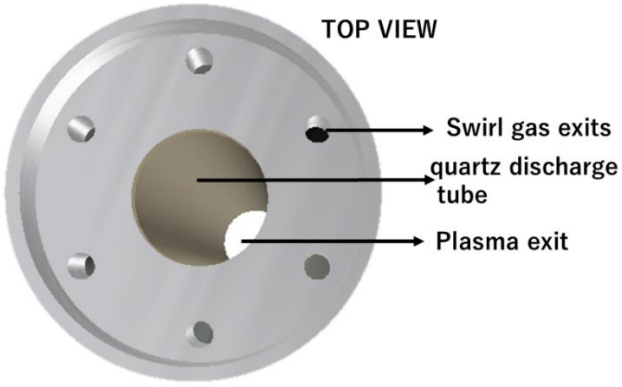

Figure 2.10 Top view of CCP device exhibiting the swirl gas exits

2.6.2.1 Dependence of plume length to swirl gas

The effect of N_2 swirl gas to Ar plasma can be observed in Figure 2.11. Without swirl gas input, Ar plasma is barely visible even at high input power. Increasing the swirl gas flow rate up to 3 l/min yields to longer plasma plume length. However, at 5 l/min N_2 flow rate, the swirl gas extinguishes the plasma leading to smaller and fainter plasma plume. The longest plume of 12.9 mm is achieved at 5 l/min Ar, 3 l/min N_2, and 40 W forward power.

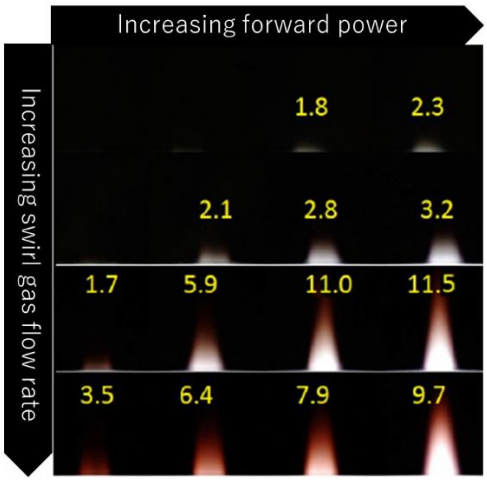

Figure 2.11 Plasma plume produced by the capacitively-coupled plasma device

2.6.2.2 Influence of swirl gas on plasma species

The spectrograph obtained from the plasma plume produced by CCP device is shown in Figure 2.12. The plasma is mainly composed of N_2 second positive system that are detected from 357 to 420 nm wavelengths and Ar I species present from 696 to 966 nm range.

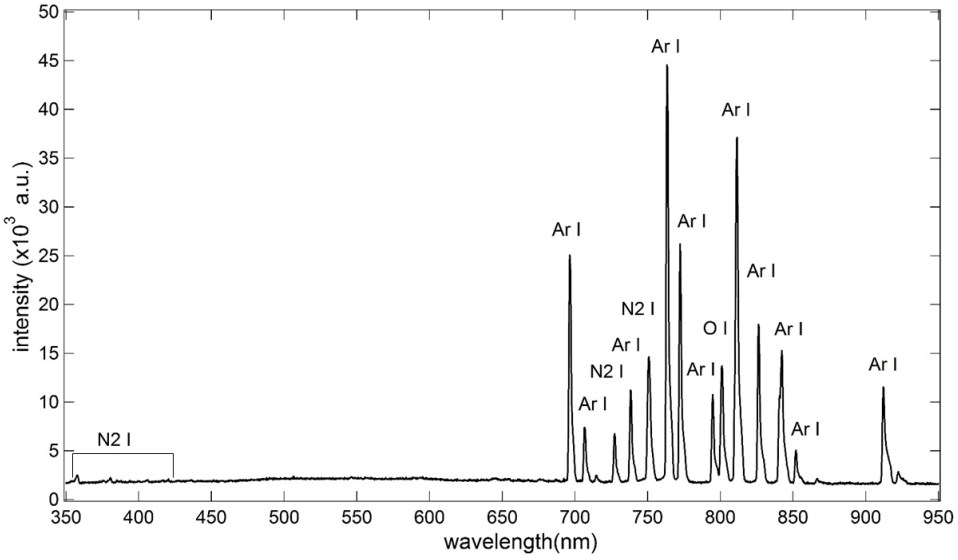

Figure 2.12 Typical emission spectrograph of the plasma produced by CCP device with swirl gas employment

To clearly see the effect of the N_2 swirl gas, the intensities of N_2 I and Ar I lines are plotted in Figure 2.13 and Figure 2.14, respectively.

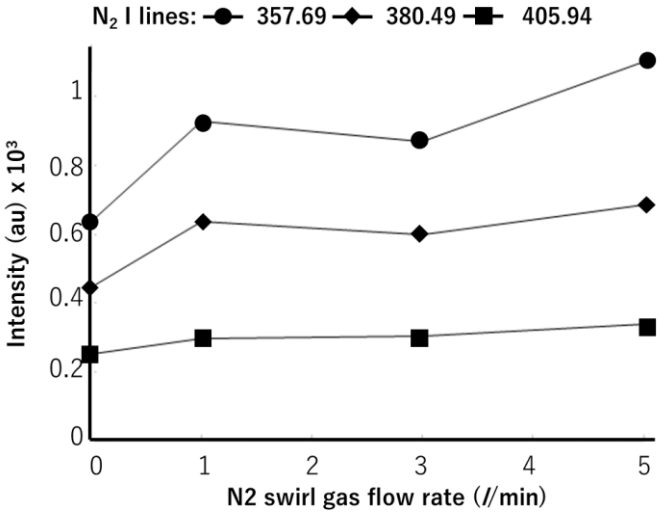

Figure 2.13 Intensities of N_2 I species for varying nitrogen swirl gas flow rate at 3 l/min Ar plasma.

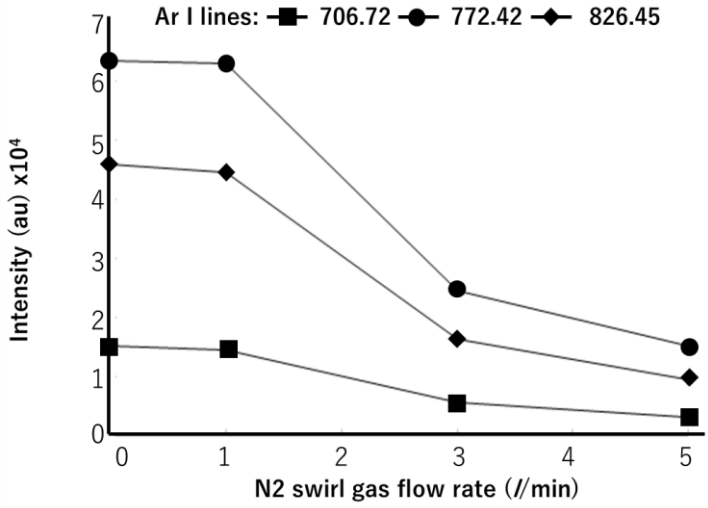

Figure 2.14 Intensities of Ar I species for varying nitrogen swirl gas flow rate at 3 l/min Ar plasma.

Since the N_2 swirl gas envelopes the plasma, some amount of nitrogen from the swirl gas mixes into the Ar plasma and is ionized when there is an increase in the N_2 gas flow rate. This in turn results in increase of molecular N_2 intensity as shown in Figure 2.13, and the decrease of Ar I species as shown in Figure 2.14 due to Ar deexcitation.

2.7 Summary

Two atmospheric pressure plasma sources, the capacitively-coupled configuration and needle-shaped electrode device successfully produced atmospheric pressure plasma plume. The obtained plume are characterized using optical emission spectroscopy and plasma glow image analysis.

The plume intensity of the needle-shaped electrode device is directly proportional to the input applied forward power and gas flow rate. Qualitatively, higher plasma density is expected as the input parameters are increased. Both atmospheric pressure plasma sources yielded N_2, Ar and O species detected through optical emission spectroscopy.

The effect of swirl gas introduction to that capacitively-coupled configuration setup is experimentally investigated through plasma glow image analysis and optical emission spectroscopy. The input of swirl gas at a proper flow rate yielded a more homogeneous plasma plume. Also, increasing the flow rate of swirl gas aids the plasma plume to be transported farther which can be optimized for specific application that would require similar plasma plume geometry.

The addition of nitrogen swirl gas into the capacitively-coupled plasma has also caused excitation of N_2 species presumably due to accompanying reduction of Ar I

species. In order to quantitatively characterize the produced plasma plume, such as positive and negative ion densities, it is necessary to develop a diagnostic method applicable for atmospheric pressure plasma theory.

Chapter 3
Gerdien condenser theory

3.1 Atmospheric charged particle measurement

The earliest electrical aerosol measurements involve the investigation of charged particles in the atmosphere and in gases exposed to ionizing radiation. The interest about charged aerosol particles yielded from the curiosity about the nature of electricity and the powerful forces it could produce in the form of lightning. A detailed history about electrical aerosol measurement is discussed by Flagan (1998).

During the 1770s, it was supposed by early investigators that the air in fine weather carries a positive charge (Chalmers 1967). Without the proper methods to measure the variation of charge with respect to the altitude, investigators at that the time did not realize that most of the positive charge is carried in the atmosphere far above the ground. Neither could the source of the atmospheric electricity be determined with the tools that were then available.

Early observations regarding the sources of atmospheric electricity and electricity transport were not understood until years later. Volta (1782) worked with Lavoisier and Laplace on a series of experiments wherein they found a number of processes that produced atmospheric electricity in gases, presumably by releasing an imbalance of charges. Volta (1782) also observed that, when a flame touched an insulated conductor

in the open air, the conductor quickly acquired charge. He asserted that this effect was not an electrical effect of the combustion because no charge accumulation occurred when the same experiment was attempted in a closed room. He associated this phenomenon with atmospheric electricity and used the technique to explore the potential gradient in the atmosphere.

Many investigators then followed Volta's measurements. Between 1810 to 1830, Schüber of Tübingen repeated Volta's measurement on the daytime variation of the atmospheric potential gradient (Flagan 1998). He also established the correlation between atmospheric potential gradient and weather (Israël 1970). Coulomb (1795) asserted that dust particle in the air were responsible for the dissipation of the electrical charge on rubbed amber. He postulated that particles of dust or air acquire charge by impact with a charged carrier and then would be repelled from it. Lord Kelvin (1859) refined the methods that had been developed in earlier investigations into the most quantitative instrument for measuring the potential gradient of the atmosphere. He then proposed continuous recording of the atmospheric potential gradient.

After the discovery of X-rays in 1895, the ability to generate charge carriers was quickly noted. The nature of gas ion was then explored more systematically. Rutherford (1897) made the connection between the atmospheric charge carriers and aerosol particles when he noted that finely divided particles in the air accelerated the loss of conductivity of the air after a source of ionization had been withdrawn. This theory has remained at the heart of ion-aerosol theory for over a hundred years. Yet there is still a need to explore the physics of air ions and their interactions with atmospheric aerosol within and beyond Rutherford's framework (Aplin 2000).

Aerosol is a collective term for the numerous particles present in the atmosphere. The size spectrum of these suspended particulate ranges from the smallest cluster ions

to relatively large particulate organic matter with radii of order 10^{-4} m. Rutherford's theory suggests that the behavior of aerosol can be inferred from observing its interaction with ions. Since, aerosol are not sufficiently charged to be deflected by weak electric fields, the electrical properties of air ions are instead studied. Ions allow the application of experimental techniques that could not be used to measure the bulk properties of aerosol. Studying ions also give insight into the formation and growth of larger aerosol particles, which have a greater direct atmospheric contact.

3.1.1 Mobility

Provided a weak uniform electric field is applied throughout a gas, a steady flow of the ions along the field lines will develop. At first sight, it might appear that an ion situated in an electric field, would experience definite force and hence would be accelerated by acquiring a velocity that would continually increase. However, the ion experiences continuous impact with the molecules of the air hence loses some or all of its momentum it has acquired since the previous impact. There will be thus an average velocity of the ion in the direction of the potential gradient (McDaniel and Mason 1973). The average velocity of the ions is called the drift velocity, v_d. The drift velocity is directly proportional to the electric field intensity E, provided that the field is kept weak.

$$v_d = \mu E \tag{3.1}$$

Where, μ is the proportionality constant called the mobility of the ions. For the lightest air ions, eqn. (3.1) is applicable only at field strengths up to 10 kV/cm (Tammet 1970). Mobility is a property of the ions and the gas through which the motion occurs. The mobility of an air ion is by definition positive for positively charged and negative for negatively charged air ions. Usually, the absolute value of μ is taken as the mobility of air ions.

3.1.2 Conductivity

The conductivity of the atmosphere is produced by ions which carry electrical charges of either sign and which move in the field. If a small potential difference is applied to two electrodes in air, a weak current flow is induced by the ions which flow in opposite directions to the electrodes where they deliver their charge. As is true in most cases of current electricity, Ohm's law is usually obeyed, and the current between two equipotential surface is proportional to the potential difference.

The current density, i, is defined as the quantity of electric charge which flows per unit time through a surface of area perpendicular to the direction of flow. Using eqn. (3.1), the current density is now given by eqn. (3.2),

$$i = \mathrm{q}(\mu^{+}n^{+} + \mu^{-}n^{-})E \tag{3.2}$$

where,

μ^{+}, μ^{-}, mobility of positive and negative ions, respectively,

n^{+}, n^{-}, concentration of positive and negative ions, respectively,

E, the strength of applied electric field,

q, the charge of the ion.

Since almost all ions encountered in the atmosphere are singly charged, the electronic charge equal to 1.602 x 10^{-19} C can be used in the eqn. (3.2). Equation (3.2) can be written as,

$$i = (\sigma_{+} + \sigma_{-})E \tag{3.3}$$

where, σ_{+} and σ_{-} correspond to the specific conductivity for positive and negative ions, respectively.

Equation (3.3) represents the case when there is only one type of positive ions and one type of negative ions. If there are ions of different mobilities with each having a corresponding density, then the above equation can be expressed as,

$$i = \sum_k (q_k^+ n_k^+ + q_k^- n_k^-)\, E \tag{3.4}$$

3.1.3 Saturation Current

Under ordinary conditions, the ionic current obeys Ohm's law and the conductivity is defined as in eqn. (3.3). However, when the supply of ions is insufficient, Ohm's law is not obeyed. Supposed a system consists of three positive ions with different mobilities, if a graph of the ionic current against the potential difference is drawn, the result will be as shown in Figure 3.1.

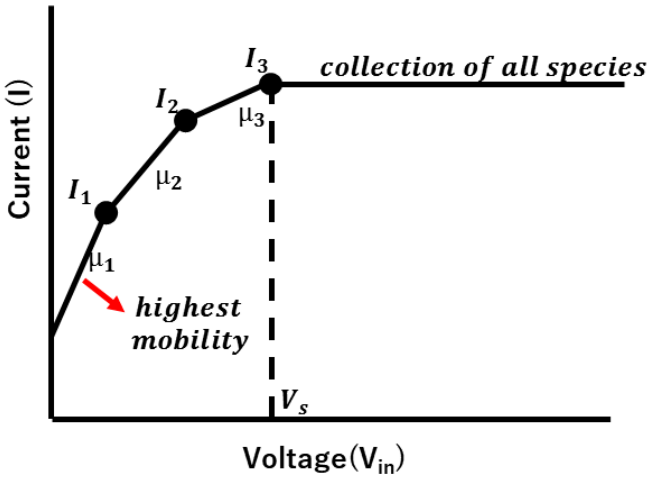

Figure 3.1 Current-voltage characteristics for multiple-constituent gas

For low values of applied voltage, there is strict proportionality with the slope and the ion mobility. However, since the number of ions are limited, saturation current will be achieved at a certain voltage V_s. From the saturation current, the total positive ion density can be calculated using eqn. (3.4) with the terms for negative ions equal to zero.

3.2 Measurement of ions using cylindrical condenser

Ions can be measured by manipulating their electrical properties such as electrostatic attraction. Hence, when subjected to electric field, ions can be counted through current measurement. The simplest way of counting atmospheric ions is by an air flowing of known velocity between two metallic plates or into a conducting cylinder with a central electrode. If an electric field is applied across the electrodes, ions will be electrostatically attracted to them. Therefore, this configuration can be considered to store charge, and is referred to as a capacitor or condenser. If voltage is applied across the electrodes of the condenser, a current can be measured which is proportional to the concentration of air ions and their ion mobility.

Measurements utilizing cylindrical coaxial condenser wherein air is drawn into the conduit is also called the aspiration method. One of the electrodes is biased to drive ions in the air stream to the other electrode. The ions collected by the outer electrode constitute a current which is proportional to the mobility of ions (Das 1993).

An apparatus with the same general principle has been used for the measurement of mobilities by Ebert in 1901 for counting of ions, and by Gerdien in 1905 for the measurement of conductivity. The apparatus consists of a hollow cylinder of radius r_o, with a smaller coaxial cylinder or wire with radius r_i. By means of a fan or pump, air is drawn through between the two cylinders with a velocity v_f. The inner cylinder or part of it, measures the ion concentration in the form of current, while a potential difference is applied between the two cylinders.

3.2.1 Development of Gerdien condenser

The Gerdien condenser has its name from one of the first constructors of ion collector instrument for measuring the air conductivity. In 1905, Gerdien developed a device which has become the standard instrument for measuring air conductivity. The air, which includes the ions to be observed, is aspirated through a cylindrical condenser. A radial electric field in the cylindrical condenser attracts one sign of ions to the collector, which can be either the central electrode or the cylinder. Information about the ion conductivities and mobilities can be obtained from the current-voltage characteristics of the condenser.

Gerdien used a cylindrical condenser with a sufficiently large air velocity to ensure that Ohm's law holds. He used an outer tube of length 56 cm and radius 8 cm, with an inner electrode of length 25 cm and radius 0.75 cm. A potential difference of 100 V was applied between the electrodes while current is measured by the inner electrode.

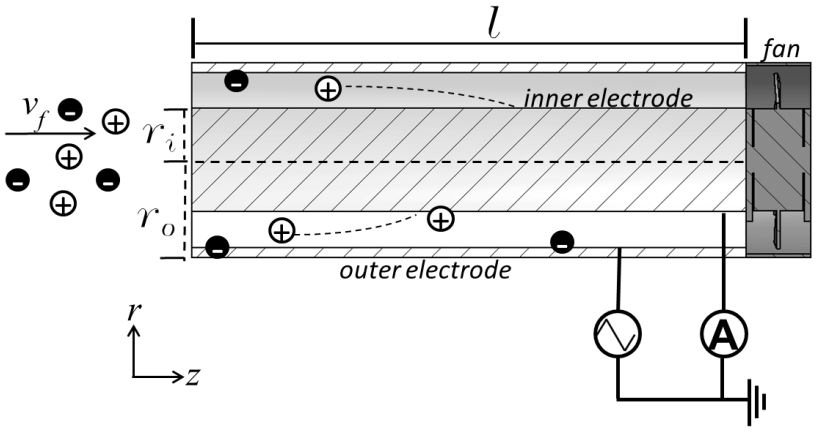

Figure 3.2 Operation principle of gerdien condenser

In Gerdien's original method, an electrometer was connected to the central electrode, which was charged to a potential V_1. After some time t, the electrometer registered a potential V_2. The conductivity was calculated from the rate of decay of the voltage across the capacitor's electrodes from V_1 to V_2. However, this technique has fallen almost completely out of use in modern implementations. Modern practice uses a constant potential difference between the electrodes and measures the current electronically. An additional application of the Gerdien condenser is that it allows measurement of different mobilities of ions through variation of the applied electric field. Some of the main difficulties with the Gerdien condenser are the effects of stray fields at the condenser opening and turbulence in the air stream through the condenser (Pedersen 1965).

3.2.2 Current-voltage characteristics

If air having positive ions of single species enters the condenser at a constant velocity v_f, the current as a function of the applied voltage V_{in} will be as shown in Figure 3.3. The current- voltage characteristic is linear until the voltage V_s reaches the value at which all of the positive ions are collected.

The saturation current collected at the inner electrode is given by eqn. (3.5) where A is the aperture area of Gerdien condenser, v_f is the velocity of ions entering the condenser, q_k is the charge and n_k is the density of ions of species k, respectively.

$$I_k = n_k q_k v_f A \tag{3.5}$$

The ion mobility μ_k is defined as the proportionality factor of an ion's drift velocity v_d in a gas and electric field strength E_r as shown in eqn. (3.6). Here, v_d gives us the radial component of the ion velocity.

$$v_d = \frac{dr}{dt} = \mu E_r \tag{3.6}$$

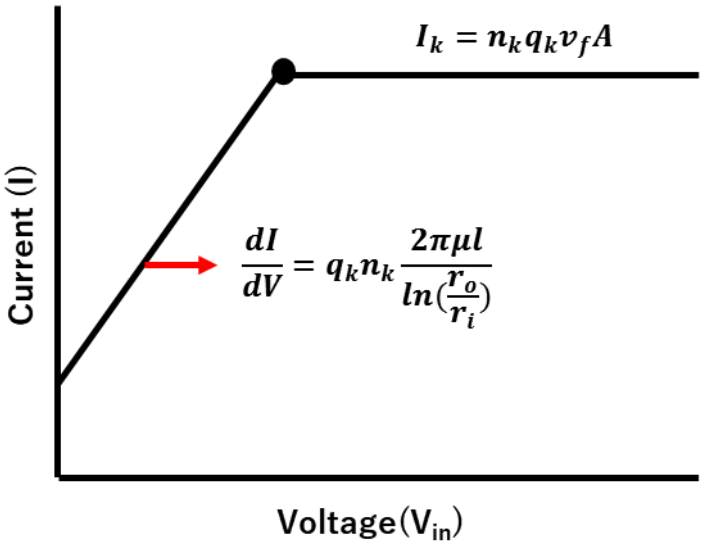

Figure 3.3 Ideal current-voltage characteristics of a Gerdien condenser

Calculating the electric field E from the electric potential V applied between the coaxial cylinder electrodes using Gauss's law, we have eqn. (3.7) to express electric field intensity in the Gerdien condenser:

$$E_r = -\frac{V}{\ln\left(\frac{r_o}{r_i}\right) r} \tag{3.7}$$

Where r_o and r_i are the outer and inner radius of cylinder, respectively. Substituting E_r to eqn. (3.6) and integrating with respect to r and t,

$$\int r dr = \int -\frac{\mu V}{\ln(\frac{r_o}{r_i})} dt \tag{3.8}$$

$$\frac{1}{2} r^2 = -\frac{\mu V}{\ln\left(\frac{r_o}{r_i}\right)} t + constant \tag{3.9}$$

Before an ion enters the cylinder, that is at time $t = 0$, condenser electrode length $z = 0$, and $r = r(0)$, where $r(0)$ is the position of ion along the radial axis, we can get a general expression for $r(0)$ given by eqn. (3.11),

$$\frac{1}{2}\left(r_{(0)}^2 - r^2\right) = \frac{\mu V}{\ln(\frac{r_o}{r_i})} t = \frac{\mu V}{\ln(\frac{r_o}{r_i})} \frac{z}{v_f} \tag{3.10}$$

$$r(0)^2 = r^2 + \frac{2\mu V}{\ln(\frac{r_o}{r_i})} \frac{z}{v_f} \tag{3.11}$$

Where the z-component of the ion velocity is just v_f. When the ions are collected at the inner electrode that is when $r = r_i$, and $z = l$, we can get the electric current flowing between the electrodes due to ions n_k from eqn. (3.5) and (3.11).

$$I_k = n_k q_k v_f \left(\pi r(0)^2\right) \tag{3.12}$$

$$I_k = n_k q_k v_f \pi (r_i^2 + \frac{2\mu V}{\ln\left(\frac{r_o}{r_i}\right)} \frac{l}{v_f}) \tag{3.13}$$

Consequently, the slope of the current-voltage (*I-V*) characteristic is given by,

$$\frac{dI}{dV} = q_k n_k \frac{2\pi\mu l}{\ln(\frac{r_o}{r_i})} \tag{3.14}$$

Equation (3.14) shows that the slope of the *I-V* characteristic of the Gerdien condenser will yield to the determination of ion mobility.

In practice, ambient air is a multiple-ion component gas. Each ion species has its own mobility, and the total current will be due to each ion species. A theoretical curve consisting of straight line segments for three mobilities is shown in Figure 3.1. The current-voltage relationship will remain linear until all ions having the highest mobility are collected. At this point, the slope of the curve will change due to saturation current

of the highest mobility ion. As the voltage is further increased, a bending point is observed in the curve at the point of total collection of each ion species of lower mobility until all ions are collected.

If the polarity of the applied voltage is reversed, the collector electrode would then collect negative charges. The same equations would hold for negative ion measurements. In addition, the current-voltage characteristics will not be changed if the collector electrode is utilized as the bias electrode and vice versa.

Also, in application, when $V_{in} = 0$, no ions are being repelled by the inner electrode hence, the total current I_T collected due to the contribution of both positive and negative ions present in ambient air is given by:

$$I_T = \sum_k K_k (q_k^+ n_k^+ + q_k^- n_k^-)\, v_f A \tag{3.15}$$

This is observed as a current offset on the *I-V* characteristics which can be caused by simultaneous collection of both positive and negative charged particles present from air inside the conduit. The total current I_T collected at this case taking into the account of the contribution of both positive and negative ions present in ambient air is supposed proportional to total current flowing into the condenser times some factor determined by diffusion or space charge K_k.

In actual measurements, due to thermal agitation and initial velocities not being uniform and not being directed entirely parallel to the condenser, the *I-V* characteristics will not break as sharply as shown in Figure 3.1 (Burt 1967.) The experimental characteristic curve will appear as shown in Figure 3.4.

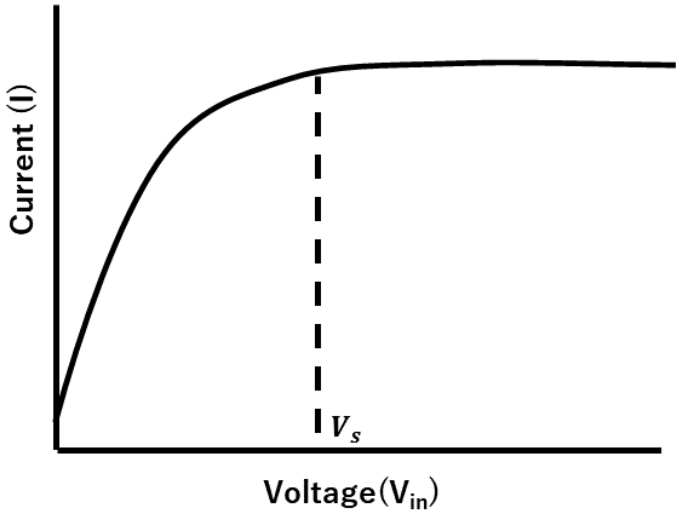

Figure 3.4 Behavior of experimental *I-V* characteristics

3.2.3 Ion mobility and density determination

We can rewrite eqn. (3.15) as,

$$I_T = qn_T v_f A \tag{3.16}$$

Where, n_T is the total ion density of all species collected. The total ion density can easily be calculated experimentally from the obtained saturation current of the *I-V* characteristics knowing the fan flow velocity and the cross-sectional area of the Gerdien condenser's conduit.

Figure 3.1 can be understood as a superposition of three different *I-V* characteristics for every ion mobility measured as shown in Figure 3.5. The saturation current corresponding to each type of ion can be estimated by subtracting the extrapolated contribution of each of the ions of lower mobility, hence providing an estimate of the density of each type of ion.

The slope S_k, which is the slope from point P_{k-1} to P_k, can be determined experimentally through a line fit in the *I-V* characteristics. The line fit of slope S_k gives

us the coordinates ($V(P_{k-1}), I(P_{k-1})$) and ($V(P_k), I(P_k)$) which are the voltage and current at point P_{k-1} and P_k, respectively

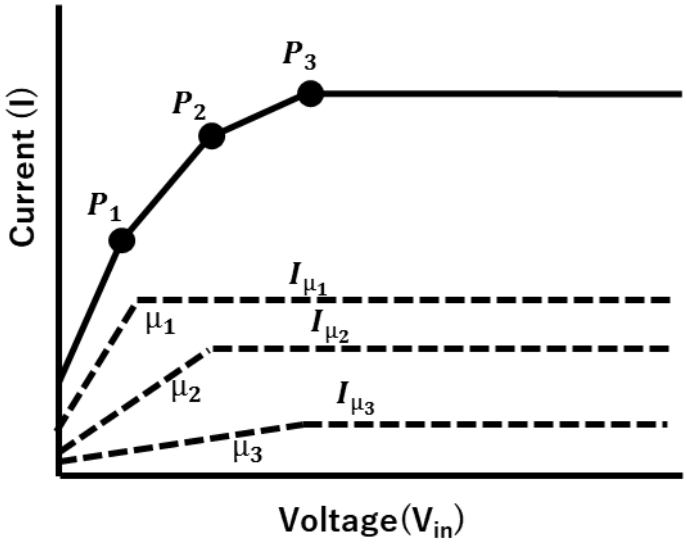

Figure 3.5 Multiple ion mobilities *I-V* characteristics and their corresponding single mobility *I-V* characteristics

In Figure 3.5, P_3 corresponds to the saturation current of ion with mobility μ_3 plus the contribution of μ_2 and μ_1 at $V(P_3)$. P_2 corresponds to the saturation current of ion μ_2 plus the contribution of μ_3 at $V(P_2)$ and so on.

In order to solve for the correct slope contribution, G_k, of each ion which can lead in the determination of ion mobility and their individual ion density, we can utilize the values of the $V(P_k)$'s and $I(P_k)$'s from the line fits of slopes S_k's, or:

$$I(P_1) = G_1 * V(P_1) + G_2 * V(P_1) + G_3 * V(P_1) \quad (3.17)$$

$$I(P_2) = G_1 * V(P_1) + G_2 * V(P_2) + G_3 * V(P_2) \quad (3.18)$$

$$I(P_3) = G_1 * V(P_1) + G_2 * V(P_2) + G_3 * V(P_3) \quad (3.19)$$

Let, matrix C, B and S be

$$C = \begin{pmatrix} I(P_1) \\ I(P_2) \\ I(P_3) \end{pmatrix} \tag{3.20}$$

$$B = \begin{pmatrix} V(P_1) & V(P_1) & V(P_1) \\ V(P_1) & V(P_2) & V(P_2) \\ V(P_1) & V(P_2) & V(P_3) \end{pmatrix} \tag{3.21}$$

$$S = \begin{pmatrix} G_1 \\ G_2 \\ G_3 \end{pmatrix} \tag{3.22}$$

In order to solve for the correct slope of each ion, the inverse of matrix B is multiplied on both sides of the equation,

$$C = BS \tag{3.23}$$

$$S = B^{-1}C \tag{3.24}$$

After solving for G_k, the density for each ion mobility can be determined using eqn. (3.25) and (3.26),

$$I_{\mu_k} = G_k V(P_k) \tag{3.25}$$

$$n_k = I_{\mu_k}/qv_f A \tag{3.26}$$

Consequently, the mobility of each ion species is given by eqn. (3.14), hence

$$\mu_k = \frac{G_k \, ln\left(\frac{r_o}{r_i}\right)}{2\pi q l n_k} \tag{3.27}$$

3.3 Gerdien condenser implementation

3.3.1 Previous work involving Gerdien condenser

The Gerdien condenser technique has been widely used in atmospheric science to identify the ion mobility, density and electric conductivity from the troposphere to mesosphere region.

Higazi *et al.* (1966) used a Gerdien condenser made of brass with 5.4 cm internal diameter and 35.6 cm long outer electrode and a 8 mm diameter and 25.4 cm long inner electrode. The outer tube was held at a suitable potential of 7 V and the current measured by the inner rod was connected to a vibrating-reed electrometer. Air was drag into the tubes by means of a vauum-cleaner fan with a flow rate of 2 *l*/sec. This device was utilized for measurements of atmospheric electrical conductivity near the ground.

Hatakeyama *et al.* (1958) developed a radiosonde instrument which consisted of a Gerdien condenser for the measurement of electrical conductivity and electric field in the upper atmosphere. The Gerdien condenser utilized by Hatakeyama (1958) consisted of a cylindrical shield with 8 cm in diameter with 30 cm length while the outer electrode is 6 cm in diameter with 26 cm length. The inner electrode is an aluminum rode of 0.5 cm in diameter and 14 cm in length.

Widdel *et al.* (1976) utilized a Gerdien probe cylinder made of aluminum electroplated with nickel. The diameter of the outer and inner electrode they utilized was 7.95 cm and 1 cm, respectively with length of 24.4 cm. The Gerdien condenser was flown into the mesosphere with a parachute to measure the concentration and mobilities of both positive and negative ions. The probe was deployed from the rocket at apogee and descended on a large parachute.

Aplin (2000) also utilized a gerdien condenser for measurements in atmospheric air consisting of a central electrode made of stainless steel wire and an aluminum cylinder as the outer electrode. A second aluminum electrode, which was connected to electrical ground so that electromagnetic interference will be reduced, was separated from the outer electrode by a PVC separator. Her miniaturized Gerdien condenser has

a length of 25.8 cm and diameters of 2.5 cm and 0.0794 cm for the outer and inner electrodes, respectively.

3.3.2 Ion mobility and density measurement

Figure 3.6 demonstrates how the experimental values of the ion mobility and density are determined from the *I-V* characteristics. Lines are fitted on the *I-V* characteristics for every change in slope observed until the saturation point (V_s,I_s) is reached. The *x* and *y* values obtained for each line fit are recorded and is entered on lines 2 and 4, respectively of the *Scilab*® code shown in Table 3.1. The *Scilab* code performs eqns. (3.20) to (3.27) discussed in Section 3.2.3. Through the code, the individual mobilities and their individual densities are determined.

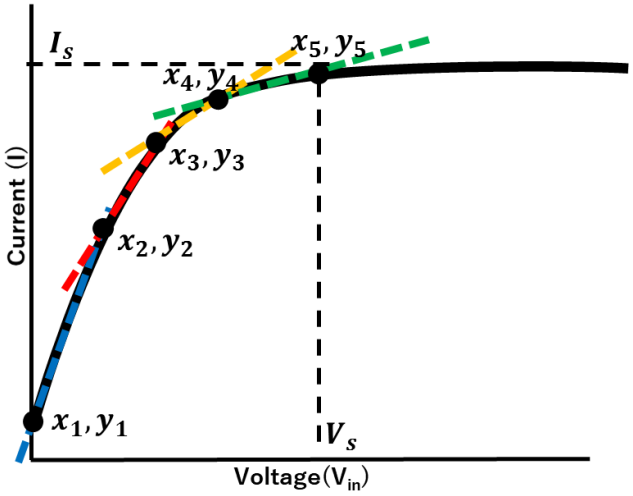

Figure 3.6 Method for density and mobility calculation

The *I-V* characteristics obtained experimentally do not have smooth curves in contrast to the graph shown in Figure 3.6. Hence, the transition points wherein the slope changes can not be easily determined. It is important therefore that before the *I-*

V characteristics are analyzed, electrical noises are filtered out from the data. A low pass filter with end pass band of 2 Hz is applied to the raw data through filter function of data analysis software *Igor* ®, then the waveforms are averaged using *Matlab*® code in Table 3.2. Finally, the *I-V* characteristics are smoothened further if needed using *Igor*.

Table 3.1 Scilab code for mobility and density calculation

```
1   //Vsat from experiment
2   Vsat=[x2, x3, x4, x5]; //sample data
3   //I from experiment, y values
4   I=[y2, y3, y4, y5]; //sample    data
5   e=1.602176565E-19; //fundamental charge
6   F=750; //fan flow rate in cm3/s
7   R=0.530628251; //ln(ro/ri)
8   L=5.9e-2; //length of Gerdien condenser
9   m=length(I); //number of slopes fitted
10  A=matrix(I, m, 1); //matrix for I from experiment
11  for i=1:m,
12      for j=1:m,
13          if j==1,
14              B(i,1)=Vsat(1);
15          elseif i==j,
16              B(i,j)=Vsat(i);
17          elseif i<j,
18              B(i,j)=Vsat(i);
19          elseif i>j,
20              B(i,j)=Vsat(j);
21  end
22  end
23  end
24  Binv= invr(B);
25  C=Binv*A; //calculating for slopes C
```

```
for k=1:m,
Isat(k)=Vsat(k)*C(k);//CALCULATE FOR REAL Isat [A]
n(k)=Isat(k)/(e*F)//CALCULATE FOR density of EACH slope [cm-3]
//mobility for each slope [cm2/Vs] from eqn. 3.27
mob(k)=abs((C(k)*R)/(2*%pi*n(k)*e*L)*10^-2);
end
```

Table 3.2 *Matlab* code for averaging the waveform

```
fnameinput ='signal.csv';%input filename here
data= importdata(fnameinput);
x = (data(:,1));
y = (data(:,2));
[allx, ~, subs] = unique(x);
ally = accumarray(subs, y, [], @mean);
finalx=allx*100; %converts to V
finaly=ally*1e-9; %converts to A
subplot(1,2,1),plot(x,y); %plots original
subplot(1,2,2),plot(finalx,finaly); %plots averaged
```

Chapter 4
Pointed inner electrode Gerdien condenser

4.1 Introduction

In this chapter, a Gerdien condenser is developed for characterization of laboratory-produced atmospheric pressure plasmas based upon the theory and operation of Gerdien condenser utilized for atmospheric science. Due to the limited dimension of atmospheric pressure plasma in laboratories, the Gerdien condenser is miniaturized to match the dimension of the produced plasma plume. The developed device works similarly with rocket-borne Gerdien condenser except that a fan is utilized as the aspirator which drag in ions into the conduit of the Gerdien condenser.

The miniaturized Gerdien condenser is modeled with reference to condenser employed in the atmosphere. The typical inner electrode for rocket-borne measurements has a conical structure at one end which helps achieve laminar air flow inside the condenser. Some examples of the Gerdien condensers for rocket-borne measurements are shown in Figure 4.1.

In contrast to Langmuir probe method which is the most common plasma diagnostic technique, the theory of Gerdien condenser is developed for atmospheric condition measurements. Also, the Gerdien condenser is non-invasive yet the plasma species present and the total ion density can be estimated. In addition, the individual

density of each ion species can be calculated from the current-voltage characteristics of the Gerdien condenser.

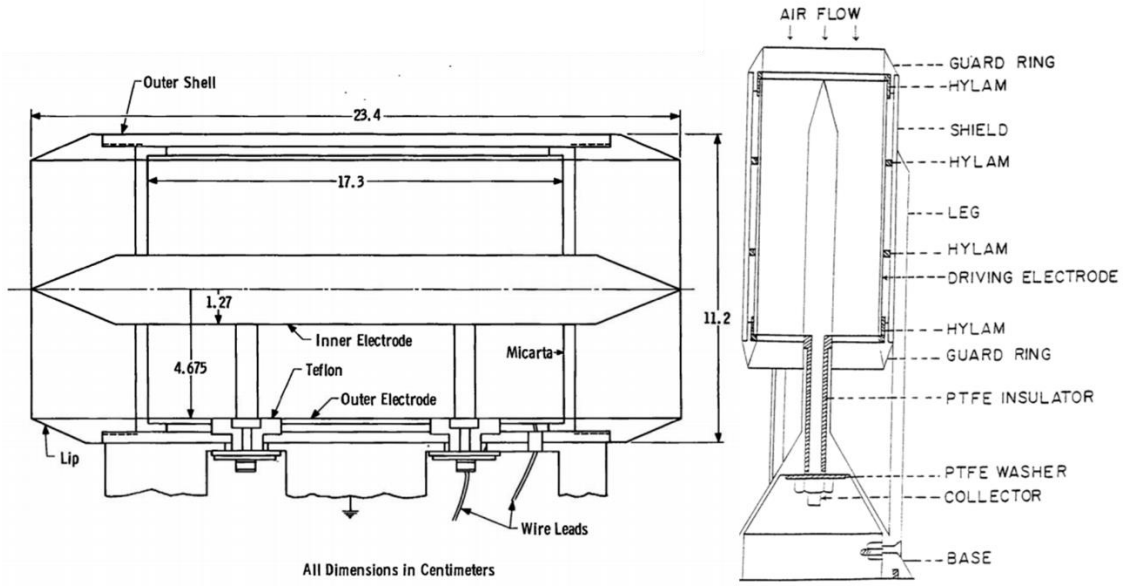

Figure 4.1 Typical Gerdien condenser for rocket-borne measurements utlized by Smith (1968): left panel and Das (1993): right panel.

The Gerdien condenser technique is advantageous for dilute plasmas which is difficult to characterized using Langmuir probe method. The miniaturized Gerdien condenser device for laboratory-produced atmospheric pressure plasma can also map the ion distribution at a distance along the axis of the ion production region. This technique can also be helpful in determining the information of the plasma characteristics for remote plasma application.

In this study, a miniaturized Gerdien condenser is tested for laboratory-produced atmospheric pressure plasma characterization. The obtained current-voltage characteristics is studied and compared to the theoretical Gerdien condenser *I-V*

characteristics. The ion density distribution along the ion production region is mapped by varying the Gerdien condenser distance to the atmospheric pressure plasma source. The positive ion species present are also determined through the calculated ion mobility from the obtained *I-V* characteristics.

4.2 Miniaturized Gerdien condenser design

Figure 4.2 shows the schematic diagram of the pointed inner electrode Gerdien condenser. The inner and outer electrodes are 55 mm and 60 mm in length, and 10 mm and 17 mm in diameter, respectively. The Gerdien condenser electrodes are both made from aluminum based on the common material utilized for rocket-borne measurements. A 25 mm x 25 mm fan is attached at the end of the condenser with a fan flow rate of 750 cm^3/s.

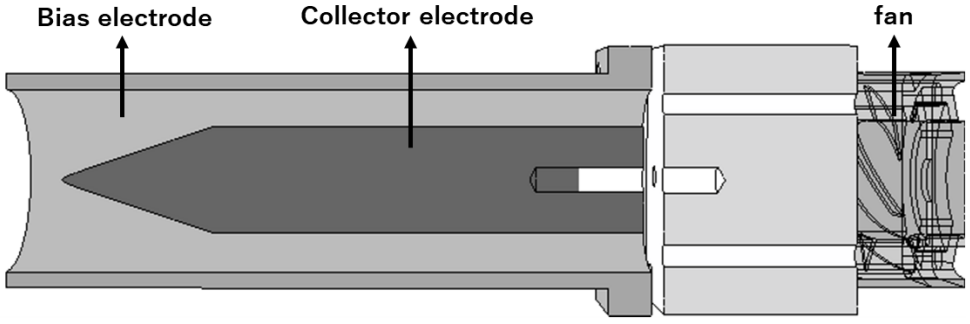

Figure 4.2 Pointed inner electrode Gerdien condenser

Although the condenser has a smaller dimensions compared to the Gerdien condensers utilized for atmospheric science, the inner electrode sharp pointed tip helps in concentrating the electric field into the current collector. The actual photo of the pointed inner electrode is shown Figure 4.3.

Figure 4.3 Actual photo of the pointed inner electrode

Shown in Figure 4.4 is the simulation of absolute electric field inside the pointed inner electrode Gerdien condenser for bias voltage of 10 V. Due to inhomogenity in the electric field at the entrance of the Gerdien condenser's conduit, positive ions are expected to be accelerated into the collector electrode therefore enhancing current measurement.

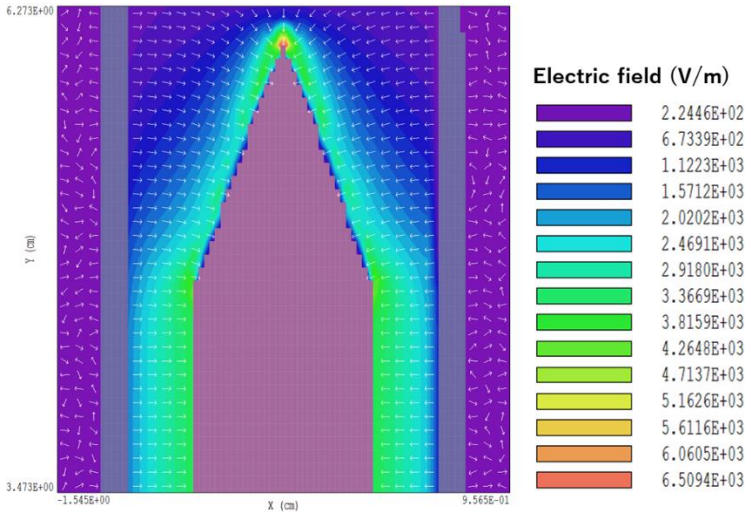

Figure 4.4 Electric field simulation inside the Gerdien condenser

However, due to the design of the collector electrode, the measurements are also prone to ambient electrical noise. In order to reduce the contribution of noise, the

measured current is post-processed by applying a low pass filter and smoothening the obtained *I-V* characteristics.

4.3 Experimental details

Figure 4.5 shows the schematic diagram of the experimental setup using the capacitively-coupled atmospheric pressure plasma device and Gerdien condenser. The CCP was successfully ignited and sustained discharge with a 13.56 MHz frequency power source at input forward power of 25 W. The impedance of the setup was tuned such that the reflected power is as low as 2 W. Flow of Ar at the flow rate of 3 liters per minute (l/min) was supplied as the main gas to produce the plasma discharge while N_2 of 3 l/min flow was used as the swirl gas to aid the plume of the atmospheric CCP out of the nozzle.

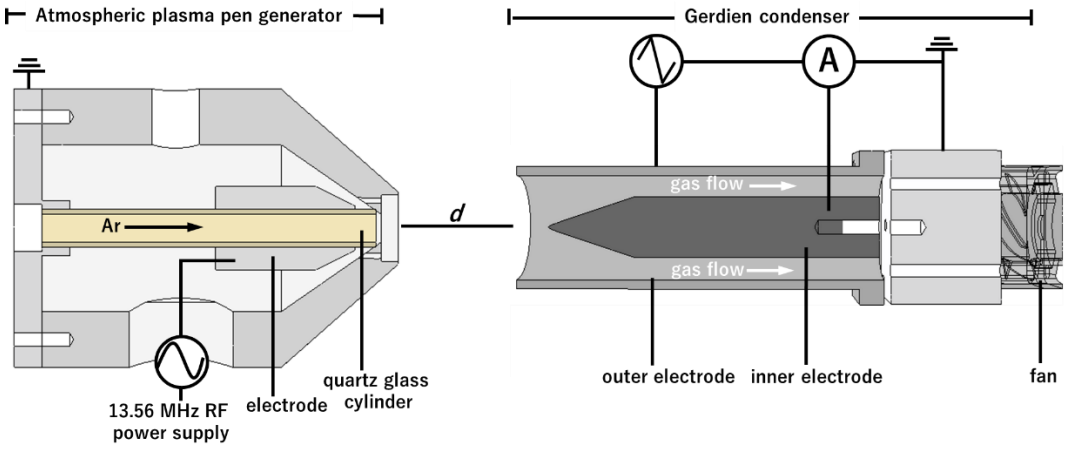

Figure 4.5 Experimental setup of pointed inner electrode Gerdien condenser

The pointed inner electrode Gerdien condenser with a 25 mm by 25 mm fan attached to its end to ventilate the tube was utilized to drag in ions into the collecting

electrode. The Gerdien condenser was positioned at the top of the plasma exit nozzle with CCP nozzle to Gerdien inlet distance varied from 5 mm to 50 mm. A triangle voltage sweep from 0 to 100 V was applied to the outer electrode to collect only positive ions. An oscilloscope was used to record the current measured from the inner electrode. The ion mobilities and their corresponding densities were calculated from the obtained *I-V* characteristics.

4.4 Implementation on capacitively-coupled APP

4.4.1 Current-voltage characteristics

Figure 4.6 shows the typical *I-V* characteristics obtained by the pointed inner electrode Gerdien condenser from the CCP. An offset on the measured current is evident when the applied voltage is equal to zero. The current offset in the *I-V* characteristics is observed for all CCP-to-Gerdien inlet distance. This offset which occurs at $V_{in} = 0$ can be caused by simultaneous collection of both positive and negative charged particles present from air inside the conduit. As the distance from the CCP nozzle to the Gerdien inlet is increased, the observed current offset decreases. This can be due to enhanced recombination of ions with the neutrals present in the air at distance farther away from the ion source.

Shown in Figure 4.7 are the *I-V* characteristics for varying CCP-to-Gerdien inlet distance. The distance of 5 mm yields the highest ion current and consequently highest ion density for each ion mobility. However, its *I-V* characteristics lacks saturation current even when the input voltage reached 100 V. The saturation region is difficult to achieve due to the fact that it is the nearest to plasma production region.

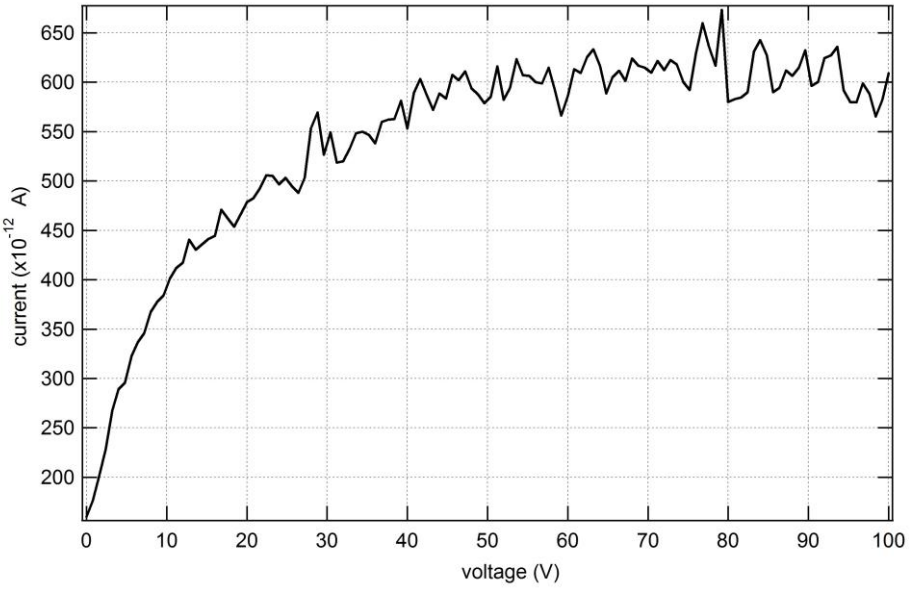

Figure 4.6 Typical *I-V* characteristics obtained by the pointed inner electrode Gerdien condenser at a distance 20 mm away from the ion source

Meanwhile, the ratio of background noise to current is observed to be high for CCP-to-Gerdien inlet distance from 40 to 50 mm. This is reasonable since the signal detected by the Gerdien condenser is inadequate. However, the slope region and current saturation of the *I-V* characteristics is still attained. An optimum CCP-to-Gerdien inlet distance is in the range of 20 to 30 mm wherein the *I-V* characteristics attains saturation current and the signal-to-noise ratio is considerably low.

4.4.2 Positive ion mobility calculation

Table 4.1 shows the calculated ion mobility and the possible ion species of the APP obtained from the *I-V* characteristics of the Gerdien condenser. The values of mobilities are compared from the ion mobility values of Ellis *et al.* (1984) and Viehland *et al.* (1995). Positive ion species such as O^+, O_2^+, Ar^+, and N_2^+ are detected to be

present at any plasma-to-inlet distance. Some of the ion mobilities calculated might be due to contribution of more than one ion species.

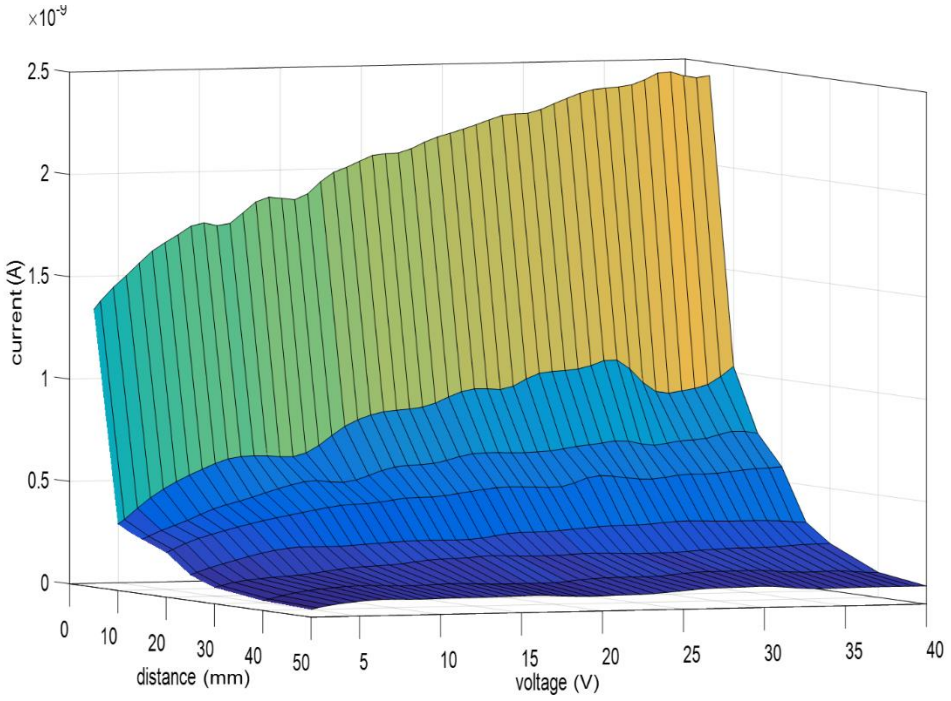

Figure 4.7 *I-V* Characteristics for varying CCP-to-Gerdien inlet distance

4.4.3 Ion densities for varying CCP–to- Gerdien inlet distance

The change in measured ion densities of some ion species for varying plasma-to-inlet distance is shown Figure 4.8. As the distance of Gerdien condenser to plasma exit nozzle is increased, the density of the ions decreases. The ion species with calculated ion mobility, μ_c of 1.99 $cm^2(Vs)^{-1}$ which yields the highest density could be mixture of O_2^+ from the ambient air and Ar^+ from the plasma discharge. The total ion density is also calculated for varying distance, *d*, which ranges from 8 x 10^5 to 2 x 10^7 cm^{-3} as listed in Table 4.2.

Table 4.1 Calculated ion mobility and the possible ion species of APP

Calculated experimental mobility, μ_e $[cm^2/Vs]$	Possible ion species
3.48	O^+
2.79	O^+
1.99	O_2^+; N_2^+
1.74	Ar^+
1.55	Ar^+
1.39	O_2^+

Table 4.2 Calculated totral ion density obtained by the pointed inner electrode Gerdien condenser

Distance (mm)	Total ion density (cm^{-3})	Distance (mm)	Total ion density (cm^{-3})
5	2.0×10^7	25	2.8×10^6
10	8.7×10^6	30	1.6×10^6
15	6.3×10^6	40	9.8×10^5
20	4.9×10^6	50	8.0×10^5

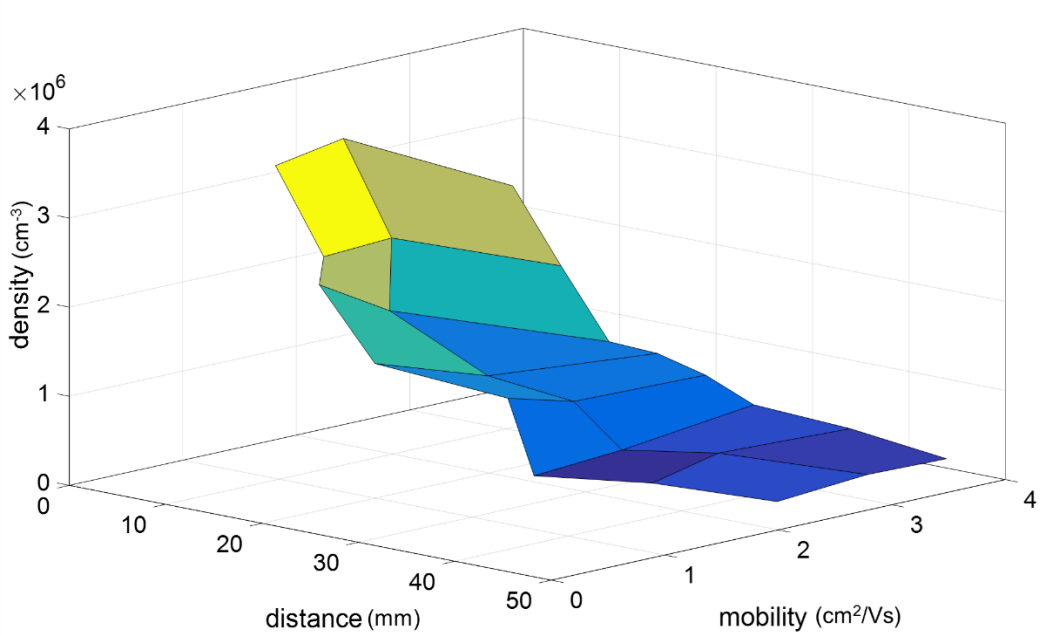

Figure 4.8 Ion mobilities and their corresponding ion densities for varying pen-to-inlet distance

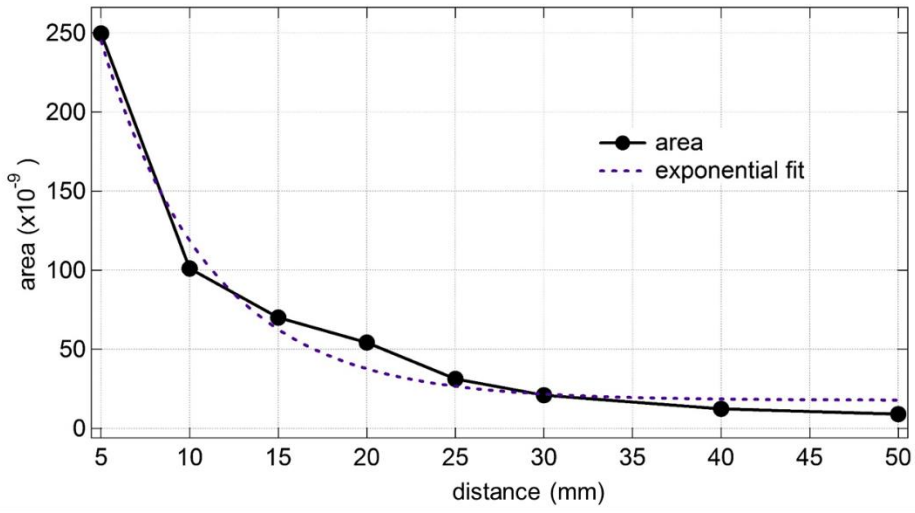

Figure 4.9 Calculated area under the *I-V* characteristics for varying CPP-to-inlet distance

Figure 4.9 shows the calculated area under the *I-V* characteristics for varying CPP-to-Gerdien inlet distance. Since the ion mobilities detected for increasing pen-to-inlet distance does not vary, the figure can be interpreted as the ion concentration distribution along the axis of the plasma production region to the Gerdien condenser. Hence, an exponential curve is fitted as also shown in 4.9.

The exponential fit has an equation of,

$$y_o + Ae^{\left(\frac{x}{\Lambda}\right)} \tag{4.1}$$

where, $y_o = 1.77 \times 10^{-8}$, $A = 5.11 \times 10^{-7}$ and $\Lambda = 0.162$. Here, Λ is the decay length of ion density as the distance from the ion source is increased.

4.5 Summary

The pointed inner electrode Gerdien condenser successfully produced signal to diagnose atmospheric-pressure plasma generated by 13.56 MHz RF power source using the capacitively-coupled configuration. O^+, O_2^+, Ar^+, and N_2^+ are identified to be present in the plasma through the calculated ion mobilities.

The ion densities of the detected positive ions are mapped for varying pen-to-inlet distance. Higher ion density could be achieved if the distance of the Gerdien condenser to the plasma exit nozzle is small. However, although 5 mm yields the highest density, saturation current is not able to be achieved. The pen-to-inlet distance from 20 to 30 mm was deduced to yield a more accurate data computation due to the large noise to signal ratio at distance higher than 30 mm.

Due to the design of the miniaturized Gerdien condenser, the noise contribution to the signal obtained are also amplified. Hence, in order to obtain more reliable estimation of ion density and mobility, it is necessary to modify the design of the pointed inner electrode.

Chapter 5
Shielded Gerdien Condenser

5.1 Introduction

A miniaturized Gerdien condenser with pointed inner electrode has been successfully utilized for characterizing the dilute atmospheric pressure plasma produced using the capacitively-coupled configuration device. In order to further improve the Gerdien condenser for diagnostics of laboratory-produced atmospheric pressure plasma, a new Gerdien condenser is designed and fabricated. One of the feature of the new version is that it employs a grounded box that is designed to shield the Gerdien condenser from unwanted signal.

It has been observed that electromagnetic interference contribute to measurement when the Gerdien condenser is exposed and a shield is not utilized. Many researchers such as Aplin (2000), Das (1993) and Hatakeyama employed an outer cylinder besides the Gerdien condenser electrodes to screen the noise that could contribute to signal measurement. The outer cylinder which is earthed is usually made of aluminum since it is light in weight, easy to fabricate and it does not require protective coating for normal use.

In this chapter, the design of the new shielded Gerdien condenser will be discussed. The insrument is also utilized for characterizing two atmospheric plasma sources that

produce dilute and dense plasma plumes. More specifically, the current-voltage characteristics and the analyzed plasma parameters produced by two different plasma sources are studied. Negative ion species are also measured by applying negative voltage to the bias electrode.

5.2 Shielded Gerdien condenser design

Shown in Figure 5.1 is the schematic diagram of the shielded Gerdien condenser. The new version has a coaxial electrodes with diameters of 1.0 and 1.7 cm for the inner and outer electrodes, respectively. Both electrodes are 5.9 cm in length and are both made of aluminum. In the new version of the miniaturized Gerdien condenser, an outer aluminum box of 2.7 x 2.7 cm in perimeter and 7.1 cm in length acts as the shield from electrical noise.

The top and bottom part of the Gerdien condenser are also shielded with a 2.7 x 2.7 x 0.5 cm aluminum box with a circular opening of 1.7 cm in diameter to let air flow on the conduit. In order to avoid unwanted electrical contact, the electrodes are fix in position using a plastic insulator made of *Delrin*. The actual images of the parts of the new condenser are shown in Figure 5.2. In order to aspirate the conduit of the condenser, a 2.5 x 2.5 cm fan with maximum flow rate of 750 cm^3/s is attached at one end of the Gerdien condenser.

5.3 Experimental details

The capacitively-coupled configuration and the needle-shaped electrode setup successfully produced plasma and sustained discharge with a 13.56 MHz frequency

power source both at input forward powers of 30 W. The impedance of the setup was tuned such that the reflected power is as low as 2 W for the capacitively-coupled configuration and less than 1 W for the needle-shaped electrode device. Gas flow rate of Ar maintained at 3 liters per minute (l/min) is supplied as the main gas to produce

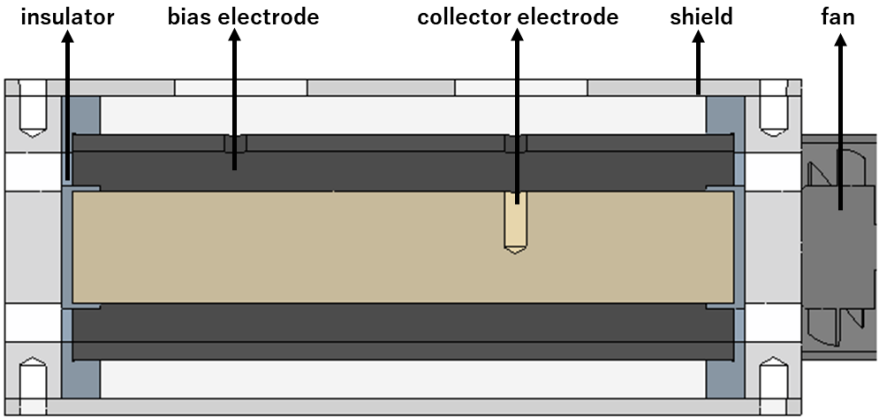

Figure 5.1 Shielded Gerdien condenser schematic

Figure 5.2 Actual photo of the shielded Gerdien condenser

the plasma discharge for both atmospheric pressure plasma sources. An additional N_2 of 3 l/min flow was used as the swirl gas to aid the plume of the APP out of the nozzle for the capacitively coupled configuration. It is important to note that the needle-

shaped electrode device produces denser plasma compared to the capacitively coupled configuration at same input RF parameters.

The shielded Gerdien condenser was ventilated by a 2.5 x 2.5 cm fan attached to its end with a fan flow rate of 750 cm^3/s. The Gerdien condenser was positioned at the top of the plasma exit nozzle with a distance of 2.0 cm. A triangle voltage sweep from 0 to +20 V was applied to the outer electrode to collect positive ions. An oscilloscope was used to record the current measured from the inner electrode. The ion mobilities and their corresponding densities were calculated from the obtained *I-V* characteristics. A negative voltage sweep was also applied to the bias electrode to test the capability of Gerdien condenser in measuring negative ion species.

5.4 Implementation on APP devices

5.4.1 Current-voltage Characteristics

Figure 5.3 shows the current-voltage characteristics obtained from the capacitively-coupled plasma and the plasma produced by the needle-shaped electrode. The difference in current magnitude is evident as the needle-shaped electrode ion source produces denser plasma compared to the capacitively-coupled configuration. In addition, the saturation current is achieved at lower voltage for the case of dilute plasma. There is also an apparent difference with the measured current offset when the applied voltage is equal to zero.

The current offset at $V_{in} = 0$ as explained in eqn. (3.15) can be caused by simultaneous collection of both positive and negative charged particles present from air inside the conduit due to either larger diffusion of positive ions or positive space

potential in the conduit. The total gas flow rate utilized in capacitively-coupled configuration is larger due to the swirl gas contribution, hence more ions are transported into the condenser's inlet.

The obtained *I-V* characteristics of the shielded Gerdien condenser is compared to the one obtained by the pointed inner electrode condenser as shown in Figure 5.4. Both *I-V* characteristics are taken from the plasma produced by the capacitively-coupled configuration setup.

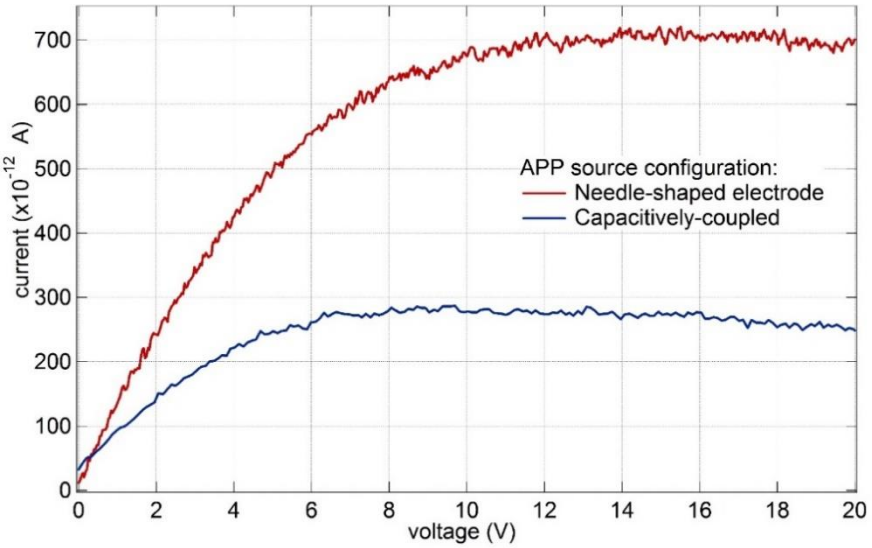

Figure 5.3 *I-V* characteristics obtained from the plasma produced by the needle-shaped electrode device and capacitively-coupled configuration setup

The difference in current magnitude as well as in current offset are also evident due to difference in the Gerdien condenser structure. If the current offset are subtracted, the pointed inner electrode still yields higher ion signal. One possibility is that the shaped of the pointed inner electrode could have enhanced the signal measurement. However, the measured current by the shielded Gerdien condenser is

noticeably smoother compared to the one obtained by the pointed inner electrode Gerdien condenser. In addition, the saturation current is easier to attain when the shielded Gerdien condenser is utilized. Given that unwanted noise could have contributed to the measured *I-V* characteristics of the Gerdien condenser with a pointed inner electrode, the measurements acquired by the shielded Gerdien condenser is more preferred.

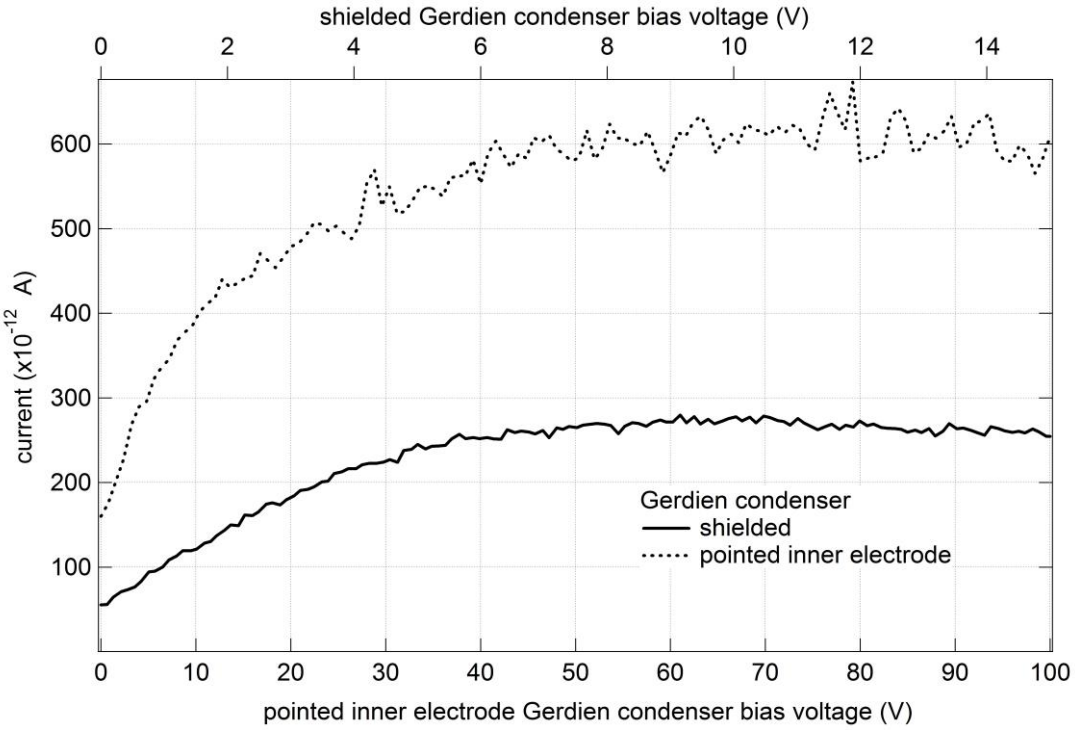

Figure 5.4 Difference in *I-V* characteristics between the two versions of miniaturized Gerdien condenser

5.4.2 Ion mobility and density calculation

Shown in Table 5.1 are the calculated mobility values from the plasma produced by the capacitively-coupled configuration and needle-shaped electrode setup.

The data are compared from the database by Ellis *et al.* (1984) and Viehland *et al.* (1995). Major part of the signal is within the range of O^+, O_2^+, Ar^+, and N_2^+.

Table 5.1 Calculated ion mobility values in cm^2/Vs and the possible ion species

Capacitively-coupled	Possible ion species	Needle-shaped electrode	Possible ion species
2.82	O^+	2.81	O^+
1.9	Ar^+,N_2^+	2.3	N_2^+
1.35	O_2^+	1.84	N_2^+,Ar^+
		1.3	O_2^+

The detected total ion density are shown in Table 5.2. The denser plasma produced by the needle-shaped electrode device has a total positive ion density more than twice of that measured from the capacitively-coupled configuration.

Table 5.2 Total ion density obtained for the two APP sources

Capacitively-coupled	2.4×10^6 cm^{-3}
Needle-shaped electrode	5.9×10^6 cm^{-3}

5.4.3 Detection of negative ion species

A negative voltage sweep is applied into the outer electrode to obtain information about negative ions present in the plasma as shown in Figure 5.5. The Gerdien condenser operation is the same even if the electric field is reversed so that negative particles are collected. Through the measured ion mobilities, O^- and O_2^- are assumed to

be present in the plasma. However, the result needs further investigation to understand the effect of electron density to the collected saturation current.

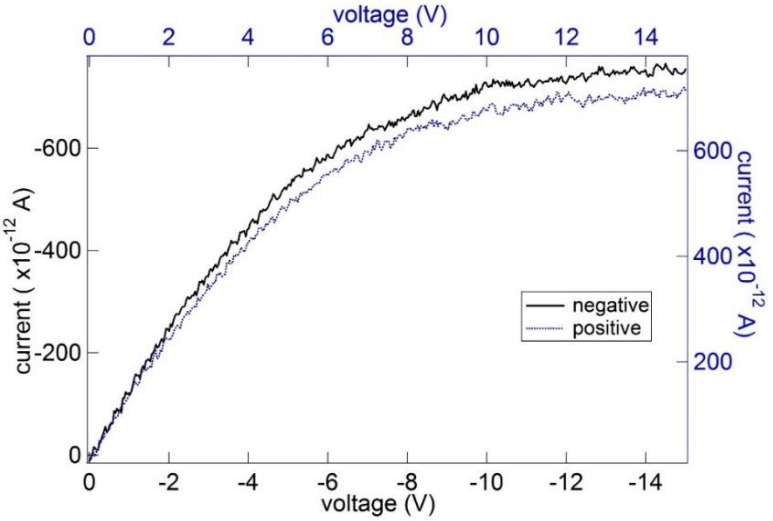

Figure 5.5 Negative ion species measurement using the shielded Gerdien condenser

5.5 Summary

The designed shielded Gerdien condenser is successfully utilized in characterizing two kinds of atmospheric pressure plasmas generated by 13.56 MHz RF power source. The current offset which has been already observed from the current-voltage characteristics of the pointed inner electrode Gerdien condenser is also detected with the new version of the Gerdien condenser. The offset is attributed to the diffusion of positive and negative ions into the conduit. Greater magnitude of current offset is acquired when the gas flow rate is higher such as for the case of the capacitively coupled configruation wherein the swirl gas flow rate is also accounted. However, further investigation is still needed such as the contribution of the electrode material work function to the current measurement.

The obtained current-voltage characteristics of the new version of the miniaturized Gerdien condenser is also compared with the one acquired by the Gerdien condenser with a pointed inner electrode. It is concluded that the new Gerdien condenser instrument yielded improved data in terms of the reduction of noise contribution to the signal.

Same ion mobilities are detected for both atmospheric pressure plasma source. O^-, O^+, O_2^-, O_2^+, Ar^+ and N_2^+ are assumed to be present in the plasma through the analyzed *I-V* characteristics.

It is also observed that the density of the denser plasma produced by the needle-shaped electrode configuration yielded more than twice of that detected from the capacitively-coupled setup due to the difference in device configuration and total gas flow rate employed.

Chapter 6
Characterization of individual components of Gerdien condenser

6.1 Introduction

The Gerdien condenser technique has been shown to give information on atmospheric pressure plasma and the results of a miniaturized Gerdien condenser for laboratory-produced atmospheric pressure plasmas are reported in Chapter 4 and Chapter 5. The miniaturized Gerdien condenser is shown to be capable of determining ion mobility with the density of atmospheric pressure plasmas from the obtained current-voltage characteristics.

In order to optimize the performance of Gerdien condenser for characterization of atmospheric pressure plasmas, the effect of its individual components are investigated. In this chapter, the flow rate of the fan attached to the Gerdien condenser is confirmed experimentally. The effect of fan flow rate to the air flow field surrounding the plasma and consequently to the measured total ion density is then discussed.

The role of the Gerdien condenser material to the acquired current-voltage characteristics is also explored in this chapter. In addition, the stability of obtained results depending upon the surface condition of the material utilized is discussed. The

origin of the droop in current-voltage characteristics is also attempted to explain in this chapter.

6.2 Fan flow rate of Gerdien condenser

6.2.1 Confirmation of fan flow rate

The fan flow rate plays an important role in analysing the plasma parameters detected by the Gerdien condenser. From eqn. (3.26), the calculated density calculation depends on the air velocity inside the conduit which is dictated by the fan flow rate:

$$n_k = I_{\mu_k}/qv_fA \tag{3.26}$$

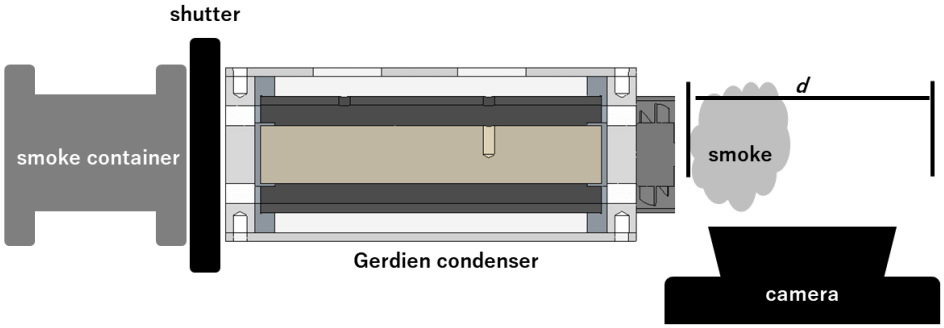

Figure 6.1 Fan flow rate confirmation experimental setup

The experimental setup for confirming the fan flow rate is shown in Figure 6.1. With the shutter closed, smoke is accumulated in a cylindrical stainless steel tube with diameter of 3.0 cm. When enough amount of smoke is stored in the tube, the shutter is opened and the smoke is dragged into the conduit of the Gerdien condenser through the fan. In this study, a *Pentax K7* camera with a speed of 30 frames per second is used to record the video of the smoke from the time it exits the fan. The fan flow rate is varied by changing the fan voltage to 4, 6, 9 and 12 V. The time it takes for the smoke to travel a certain distance, *d*, after exiting the fan is calculated through image analysis using *imageJ*.

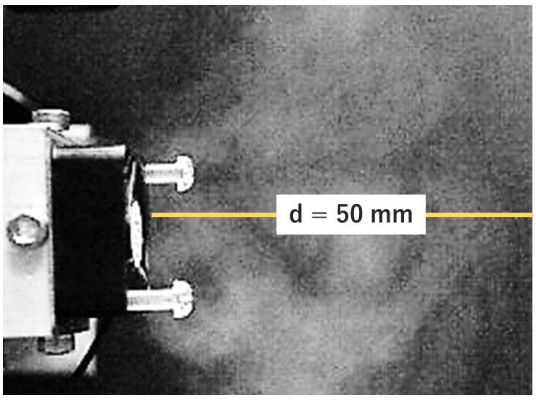

Figure 6.2 Actual image obtain during fan flow rate confirmation experiment

Listed in Table 6.1 are the experimental flow rate and the flow rate from the manufacturer's catalogue. The deviation is computed to be less than 6%. Hence, for all calculations, the value of fan flow rate as provided by the manufacturer is utilized.

Table 6.1 Experimental values of fan flow rate

Fan voltage (V)	Experiment Flow rate cm^3/s	Catalogue Flow rate cm^3/s	Deviation (%)
4	236	250	6
6	354	375	5.7
9	566	563	5.3
12	766	750	2.1

6.3 Effect of air velocity to current-voltage characteristics

In this study, the influence of fan flow rate to the detected plasma parameters of the Gerdien condenser is investigated. The plasma produced by the needle-shaped

electrode setup and the capacitively coupled configuration are studied as the fan flow rate is varied from 190 to 750 cm^3/s for fan voltage of 3,6,9 and 12 V. The plasma plume for both ion sources are produced using the 13.56 MHz RF power supply at input forward power of 30 W. Both sources utilized an Ar gas with 3 l/min while an additional N_2 swirl gas of 3 l/min is used for the capacitively coupled configuration.

Shown in Figure 6.3 are the current-voltage characteristics acquired from both APP sources. As discussed in Section 5.4.1, higher flow rate yielded higher current offset. Hence, as the fan flow rate is increased, the current obtained when the applied voltage is zero also increases.

In addition, the current magnitude is observed to increase for higher fan flow rate. The increase in fan flow rate affects the air flow field surrounding the plasma. This results in enhanced ionic recombination among species of the plasma in the ambient air, hence a decrease in the detected total ion density is observed. However, the detected density did not decrease in proportion to the fan flow rate. The smaller input gas flow rate of the needle-shaped electrode device should create an air flow field of faster recombination rate at the region between the Gerdien condenser and the APP devices.

Table 6.2 Measured ion densities 2.0 cm away from the APP inlet at varying Gerdien fan flow rate.

Fan flow rate	Ion density, n [$10^6 cm^{-3}$]	
[$10^2 cm^3 s^{-1}$]	Capacitively coupled	Needle-shaped electrode
1.9	4.1	16.2
3.8	3.1	8.6
5.6	2.8	6.7
7.5	2.4	5.9

The denser plasma produced by the needle-shaped electrode device yielded higher ion density ranging from 6 to 16 x 10^6 cm^{-3} compared to the capacitively coupled configuration with ion density from 2 to 4 x 10^6 cm^{-3}.

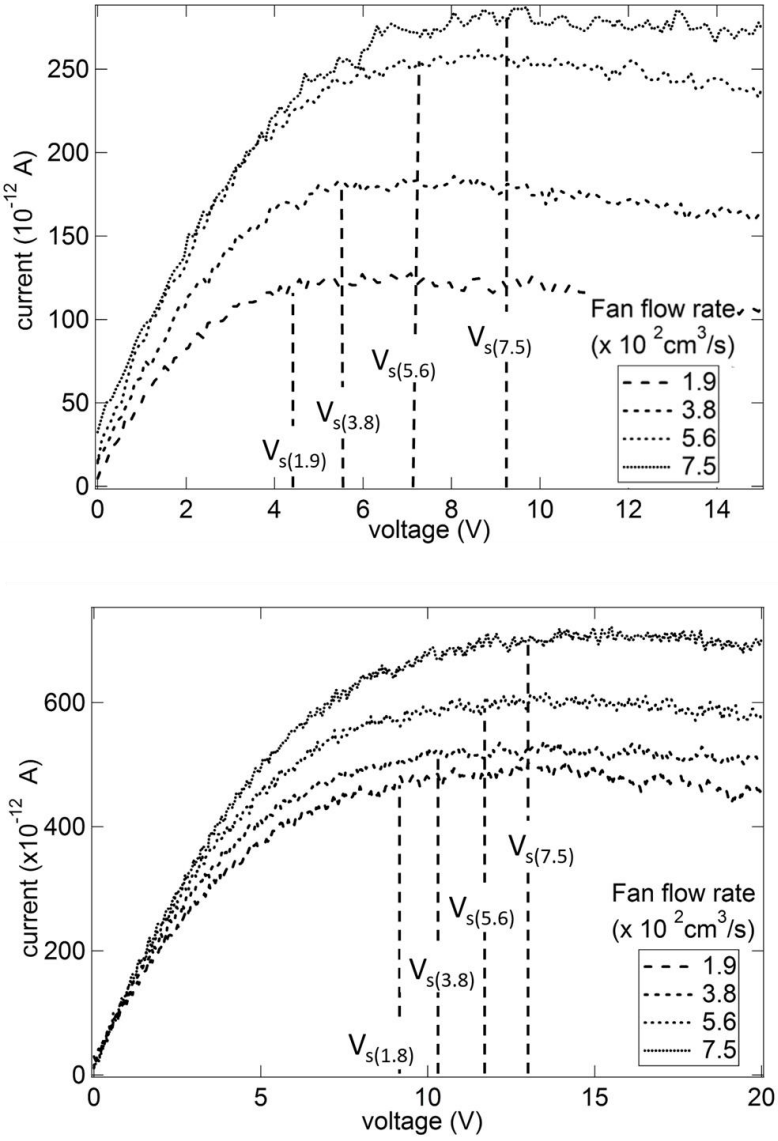

Figure 6.3 *I-V* characteristics produced by Gerdien condenser for the measured plasmas of capacitively coupled configuration [top] and needle-shaped electrode device [bottom] at varying fan flow rates. The dash lines mark the start of current saturation.

6.4 Effect of material to Gerdien condenser performance

6.4.1 Introduction

It has been shown that the increase in fan flow rate affects the air flow field surrounding the plasma resulting to a decrease in detected total ion density. One factor that should possibly affect the measured *I-V* characteristics is the electrode material. Aging has been a normal phenomenon for electrode material which causes discrepancies on its performance. Baglin (2000) reported that the technical materials utilized for particle accelerators yields different results due to the effect of oxide layer and of the adsorbed water on the surface. Work function of metal surface can change depending upon adsorbate, while the change alters potential difference between electrodes of the condenser. Thus, the effects of the individual electrode component are to be investigated in order to optimize the capability of Gerdien condenser for characterization of atmospheric pressure plasmas.

The most common material used to make Gerdien condenser devices is brass following the successful use of the material for ion mobility measurement. However, for utilization with radiosondes, the Gerdien condenser device has to be made of durable against surface oxidation and light weight materials such as aluminum. Aplin (2000) briefly discussed about the effect of tube material but only on chemical reactivity. She preferred stainless steel to aluminum as a more reliable electrode material. Wahlin (1989) reported that the electrode material causes an offset on the *I-V* characteristics which is due to the contact potential difference of the material. Meanwhile, Harrison *et al.* (2000) suggests that the change in temperature affects the variation in voltage offset. Some researchers suggested voltage offset values to counteract the current offset depending on the material. For example, Wahlin (1989) suggested that copper should

be biased at -0.45 V while aluminum at -1 V bias. Hatakayema applied an offset of -140 mV for aluminum, however they did not explain how the quantity was obtained.

Another solution was to plate the electrode with a more stable material. Rose *et al.* (1972) applied nickel plating to aluminum after they have observed that the shift in the *I-V* characteristics may be caused by the insulating oxide layer which is always present on untreated aluminum surface. Meanwhile, Das (1993) utilized a brass electrode electroplated with nickel for a polished corrosion free surface. However, there is no report if the observed offset on the *I-V* characteristics diminished after plating the electrode. Although some researchers suggested different solutions to counteract the current offset, the effect of the electrode material has not been comprehensively investigated. It is important to analyze the effect of the electrode material to the *I-V* characteristics for more reliable treatment of data to deduce plasma parameters by using a Gerdien condenser.

6.4.2 Experimental details

The atmospheric pressure plasma source in capacitively-coupled configuration is used in this study. The APP were ignited and sustained at 30 W forward input power. Typical reflected power to the source did not exceed 1.5 W. A flow controller regulates Ar supply to the generator at 3.0 liter per minute. However, N_2 swirl gas is not introduced into the system in order to isolate the possible effect of nitrogen ion species interacting with the surface of the Gerdien condenser electrode.

6.4.2.1 Gerdien condenser operation

Three pairs of inner and outer electrodes, specifically made of aluminum, copper and nickel, were initially polished using 600 and 1200 abrasive papers, and then rinsed

with ethanol. The assembled Gerdien condenser was positioned 2.0 cm away from the plasma exit nozzle. A voltage sweep from -20 V to 20 V was applied to the outer electrode while the current was measured at the inner electrode. An *I-V* characteristic was recorded 15 minutes after polishing and assembling the Gerdien condenser of each electrode material. Traces were subsequently recorded after every 30 minutes over the period of 3 hours. Images of the inner electrodes before and after the operation were taken using an optical digital microscope (*Shodensha TG500PC2 5.0 megapixel USB microscope*).

6.4.3 Current-voltage characteristics

Figure 6.4(a) shows the raw data of the applied voltage to the outer electrode with sweep duration of 20 seconds and the typical current behavior measured by the inner electrode of the Gerdien condenser as a function of time. Substantial amount of the displacement current is observed when the voltage sweep rate of the bias electrode exceeded about 8 V/s. After subtracting the displacement current for sweep durations of 0.1 and 5 seconds, the measured *I-V* characteristics are nearly identical as shown in Figure 6.4(b). Hence, the voltage sweep time duration is set to 20 seconds in this study to eliminate contribution from displacement current onto the measured *I-V* characteristics.

Noise arising from atmospheric pressure discharge is filtered out through a low pass filter with end pass band of 2 Hz then the *I-V* characteristics are smoothened. It is important to note that there is asymmetry between *I-V* characteristics of positive and negative ions for higher voltages as shown by the inset in Figure 6.4(b). The difference in the slope region and on the saturation current is due to the difference in the ion

species collected by the Gerdien condenser depending upon the polarity of the applied voltage. Further discussion on ion mobility and density is included in Section 6.4.7.

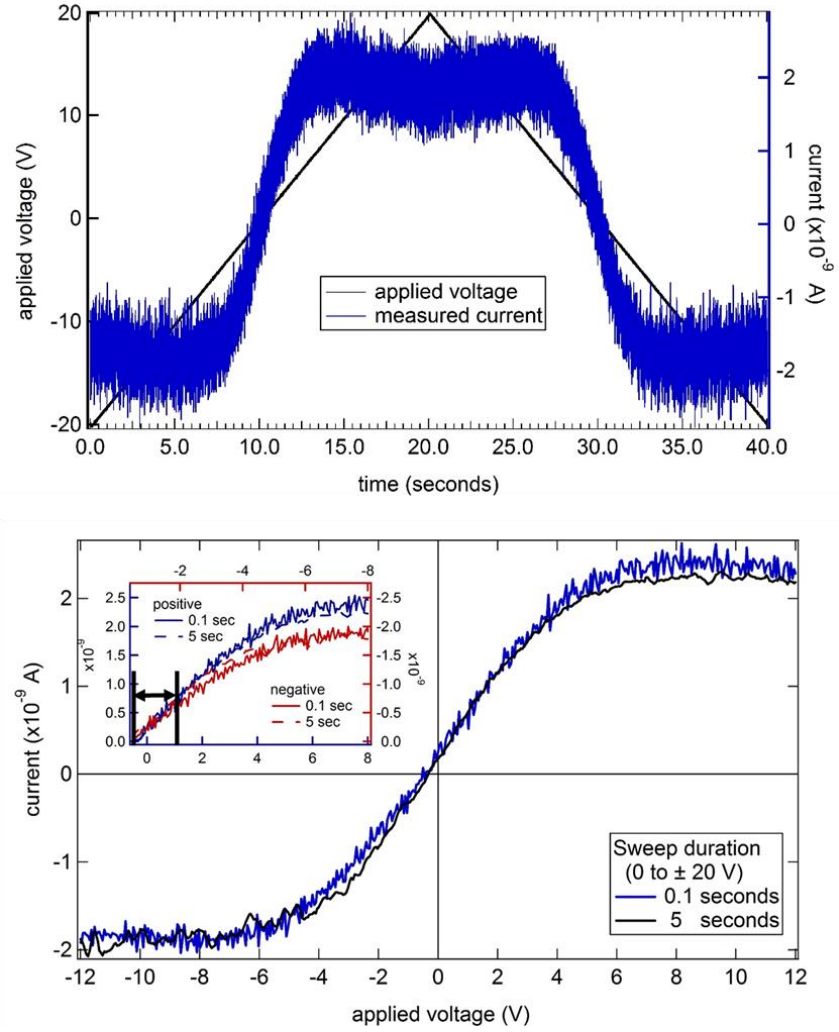

Figure 6.4(a) Raw data of bias voltage with 20 seconds sweep duration and measured current as a function of time and (b) *I-V* characteristics for bias voltage sweep duration of 0.1 seconds and 5 seconds after subtracting the effect of displacement current.

Shown in Figure 6.5 are the *I-V* characteristics after smoothing. They are acquired using the fresh electrodes and 180 minutes after exposure to ambient air. Each material exhibits a unique *I-V* characteristics behavior as depicted in Figure 6.5.

The acquired ion current indeed showed dependence upon the change in the electrode surface condition hence different results are obtained when the material is varied. Initially when the electrode surfaces are freshly cleaned, all the materials exhibited similar saturation current, I_{sat} when the applied voltage is positive to let the collector electrode to detect positive ions.

However, when the bias voltage is negative, the obtained I_{sat} deviated significantly depending upon the electrode material. The largest positive I_{sat} is measured for copper electrode while the lowest current is measured for nickel. After exposing the electrodes to ambient air for about 180 minutes, I_{sat} dropped for both positive and negative ion measurements. However, the amount of the current drop is larger for negative ion collection, where copper electrode recorded a decrease by 33 %. For positive ion collection, the largest drop in I_{sat} is 4 x 10^{-10} A which is observed for aluminum electrode. The obtained values of I_{sat} are listed in Table 6.3. It is surprising to observe, that negative saturation currents are completely different from the fresh electrode surface condition, while the positive saturation currents for three electrode materials are similar for fresh electrodes.

6.4.4 Electrode potential

Another distinct difference observed in the *I-V* characteristics is the shift in the electrode potential, ΔV, defined as the bias voltage when the measured current is equal to zero. The electrode potential varies depending on the material, resulting in different shifts in *I-V* characteristics on the abscissa.

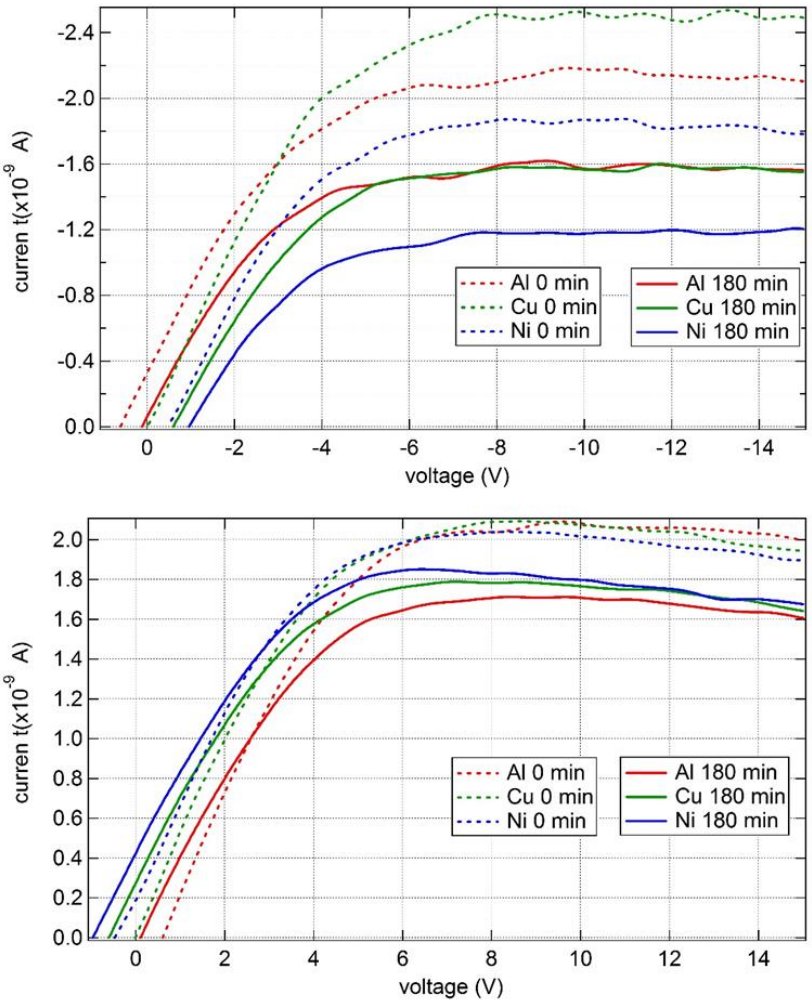

Figure 6.5 Current-voltage characteristics obtained for measurement of (a) negative and (b) positive ions using fresh electrodes and 3 hours after exposure to ambient air.

Clear differences between fresh and atmosphere exposed electrodes are easily seen in Figure 6.6, which shows the entire *I-V* characteristics during a voltage sweep for nickel electrode. First, the drop in saturation current for both negative and positive measurement is evident. Secondly, the *I-V* characteristics shift according to the change in electrode potential which is observed to be an effect of long exposure to ambient air.

Table 6.3 Saturation current measured from the *I-V* characteristics.

	I_{sat} [-1 x 10^{-9} A] (negative bias)		I_{sat} [1 x 10^{-9} A] (positive bias)	
Material	0 min	180 min	0 min	180 min
Al	2.2	1.6	2.1	1.7
Cu	2.4	1.6	2.1	1.9
Ni	1.7	1.2	2.1	2.0

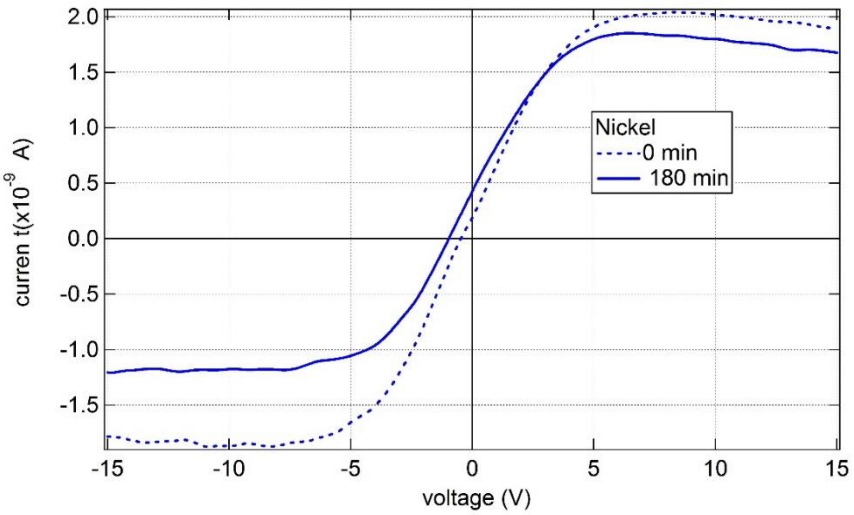

Figure 6.6 *I-V* characteristics of nickel from -15 to 15 V sweep.

6.4.5 Change in surface condition

The decrease in measured saturation currents and shift in voltage which are exhibited by all materials suggest that there is accumulation of adsorbates on the electrode surface affecting the current collection by the electrode, and surface potential barrier. Shown in Figure 6.7 are the images of the electrodes before and after exposure

to ambient air. Although copper exhibited the most noticeable surface change, aluminum and nickel also displayed a varied surface condition visible to the naked eyes. It is presumed that the adsorbates that have developed on the electrodes are oxide layers that occurs naturally on an exposed metal surface but with patterns relevant to ion collection.

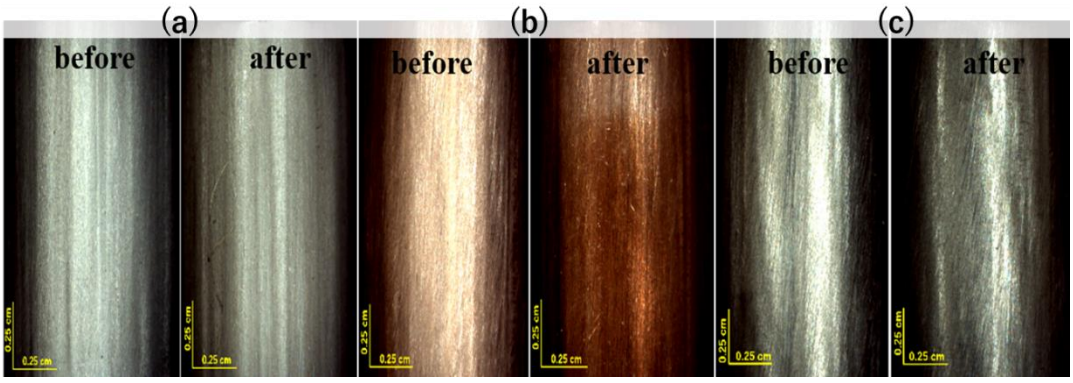

Figure 6.7 Images of (a) aluminum, (b) copper, and (c) nickel electrodes before and after exposure to ambient air.

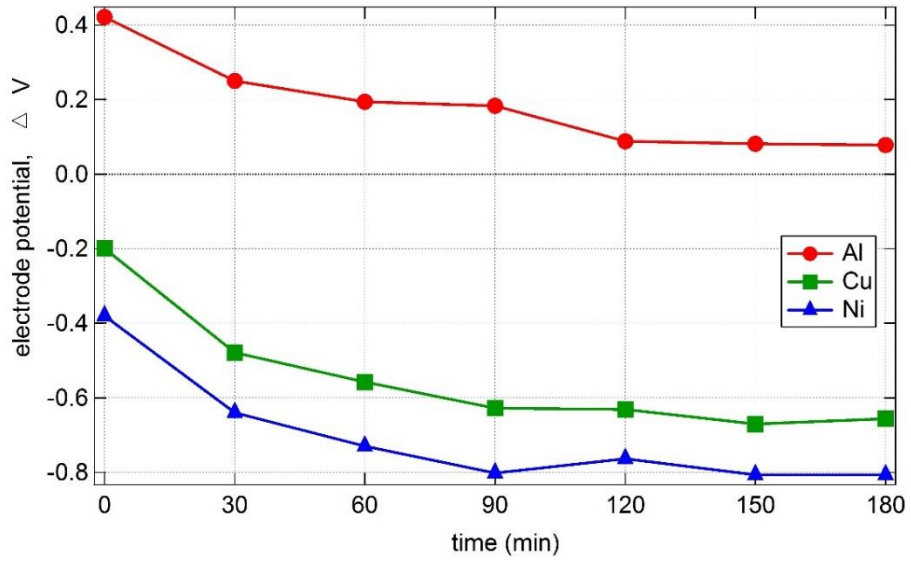

Figure 6.8 Change in electrode potentials of all materials utilized over time.

Shown in Figure 6.8 is the graph of electrode potentials of all materials as function of time. For all materials, the electrode potentials approached to values more negative than the initial values. They tend to saturate after around 90 to 120 minutes. Only aluminum yielded a positive offset on *I-V* characteristics for both initial and final trace. Both copper and nickel have negative electrode potentials initially, but nickel exhibited the most negative value.

Surface properties like work function should mainly determine the electrode potential. Wahlin (1989), for example, discussed that the effect of contact potential is eliminated since Gerdien condenser comprises of electrodes of the same material. However, since the surface conditions of inner and outer electrodes become different due to exposure of ion current at different current density, we may observe asymmetric saturation current. The asymmetry also enlarges as the exposure to APP, which is consistent with the progress of surface modification by charged particles/oxidation. On the other hand, there can be also a contribution due to space charge inside of the condenser. The electrical contact potential difference between the electrodes is also relevant to the oxidation chemical potential of the material. Since aluminum has the highest tendency to oxidize, it can develop the most passivated surface compared with other two materials.

6.4.6 Stability

Stability in *I-V* characteristics is necessary for reliable analysis; if we know how the aging of the collector electrode develops, we do not have to polish the electrode every time but utilize "saturated" electrode. To examine the stability of each material over time, the change in the area under the *I-V* characteristics is calculated and plotted as shown in Figure 6.9. The area is obtained by integrating the current from the

obtained ΔV to ± 20 V. From this figure, an exponential curve is fitted and the time constant for each material are derived as listed in Table 6.4.

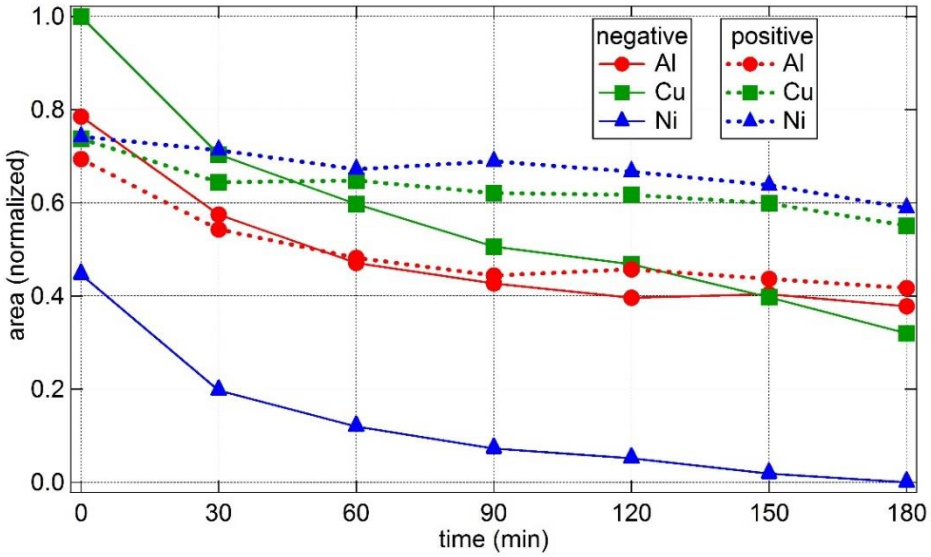

Figure 6.9 Area under the *I-V* characteristics from the measured electrode potential to ±20 V.

Table 6.4 Time constant calculated from exponential curves fitted in Fig. 7.

Material	Positive bias	Negative bias
Al	36.6	40.6
Cu	99.6	70.4
Ni	----	40.7

The measurements obtained using aluminum electrode seems to achieve saturation for both positive and negative ion measurements with reasonably fast time constant. On the other hand, the *I-V* characteristics obtained using copper continued to

decrease for both positive and negative ion collection. Nickel yielded most stable positive ion measurements but the current measured during negative ion collection decreases with the characteristics similar to aluminum.

6.4.7 Ion mobility and ion density

Figure 6.10 shows the detected positive and negative ion mobilities and their corresponding density. The individual ion densities are evaluated similar to the method discussed by Burt (1967). The uncertainties shown in the figure are from the variation of mobility and density values calculated from the three materials utilized. All the materials yielded similar negative and positive ion mobilities which are identified to be those of Ar^+, Ar^{++}, N^+, N_2^+, O^+, O-, O_2^+ and O_2^-. Hence, the detected ion species are not dependent on the electrode material utilized. The negative ion mobility around 5.0 cm^2/Vs may be due to electrons, while 1.5 cm^2/Vs may be due to negative ion cluster which is yet to be identified. To observe the effect of change in surface condition, the ion mobility is also derived after long exposure to ambient air.

The ion mobilities are observed to shift possibly due to the shift in electrode potential. Hence, in order to obtain an ion mobility spectrum with the effect of electrode potential eliminated, the *I-V* characteristics can be shifted accordingly.

Listed in Table 6.5 are the calculated total positive and negative ion densities for all materials measured before and after exposure to ambient air. The total ion densities are calculated using the same method as discussed in Chapter 3. Parallel to I_{sat} behavior in Section 6.4.3, the same positive ion density is attained only when fresh electrodes are used. The highest negative ion density is attained when fresh copper electrode is utilized. After the 3-hour period, the measured densities for both positive and negative ions were observed to decreased. Nickel tends to favor positive ion collection resulting

to the highest positive ion density measured. Correspondingly, nickel yielded the lowest negative ion density measured even when fresh electrodes are used.

Table 6.5 Total ion densities of positive and negative ions detected by the Gerdien condenser.

	Negative ion density [1 x 10^7 cm^{-3}]		Positive ion density [1 x 10^7 cm^{-3}]	
Material	0 min	180 min	0 min	180 min
Al	1.8	1.33	1.75	1.42
Cu	1.99	1.33	1.75	1.58
Ni	1.42	1.0	1.75	1.66

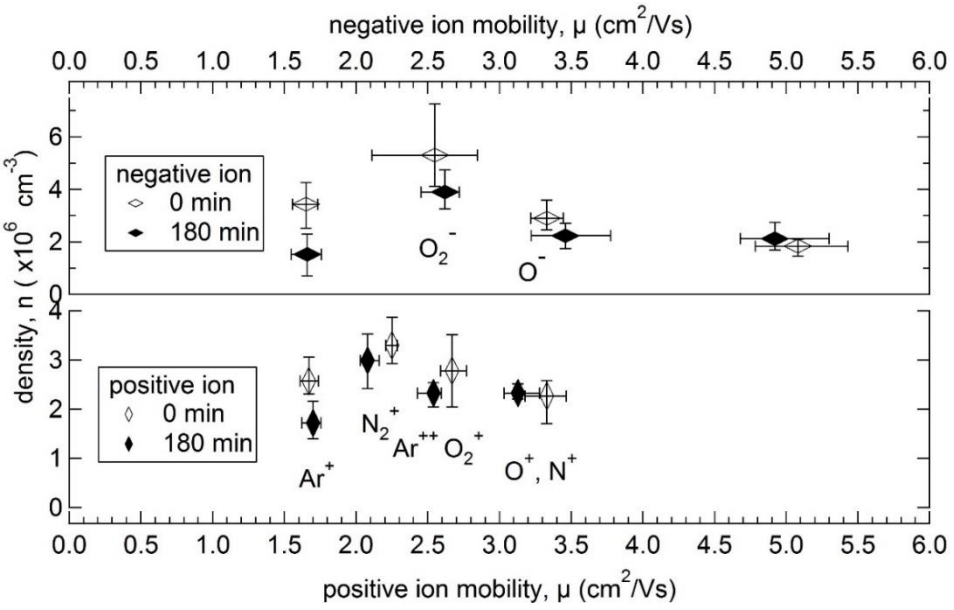

Figure 6.10 Ion mobility derived before and after 180 min exposure to ambient air by applying negative[top] and positive [bottom] bias.

6.5 Investigation of electrode edge effect to *I-V* measurement

6.5.1 Introduction

The theory used for solving the ion mobility and density assumes that the electric field inside the Gerdien condenser is independent of axial distance, that is, the calculation is based upon the assumption that the condenser is infinitely long. However, for a condenser of finite length, the electric field distribution is modified at the ends of the electrodes. As a result, all electric field lines originating from the bias electrode do not terminate at the collector electrode. This occurrence is called the edge effect.

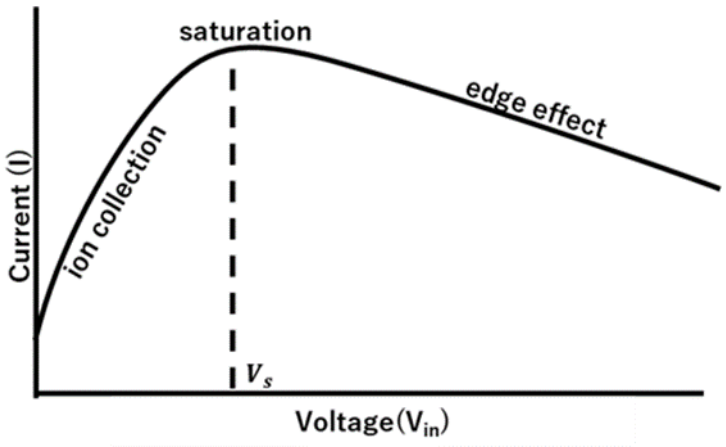

Figure 6.11 Edge effect visualization on the current-voltage characteristics

The electric field strength and configuration at the front opening of the condenser have a controlling effect on incoming ions or electrons. Hence, the collecting area of the condenser depends on the strength of the electric field along the radial axis. Schmeer and Hock showed that for large applied voltage, the saturation current decreases instead of remaining constant. This is due to the electric field lines of force originating from the surface of outer cylinder have a repelling effect on arriving ions.

Some of the solutions done in eliminating the edge effect is by introducing a third cylinder that is grounded which then acts as a shield so that electric field lines originating from the outer surface of the bias electrode do not end into the collecting electrode. Another solution suggested is to closed both ends of the condenser electrode with a wire mesh. By doing so, the field lines will not extend outside the wire mesh. However, (Rose and Widdel 1972) have reported that this method reduces the collection efficiency of the instrument by more than 50 percent.

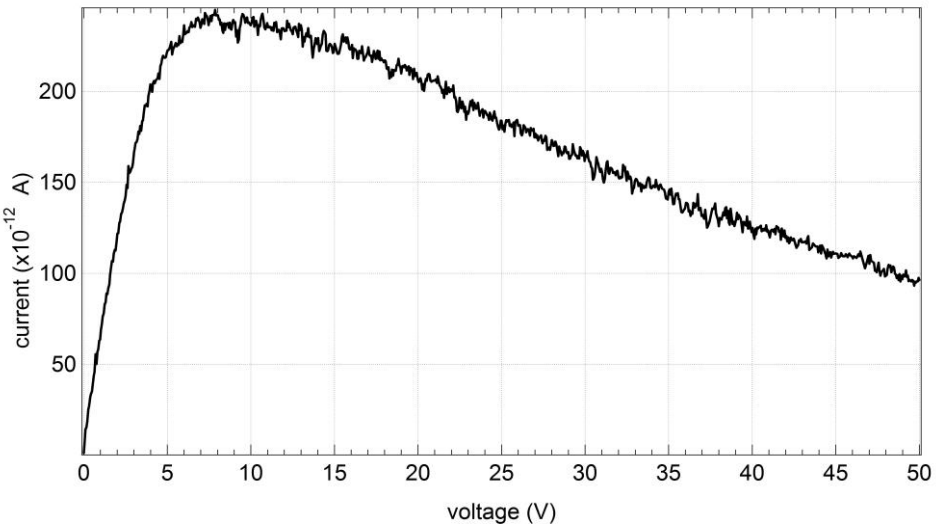

Figure 6.12 Experimental *I-V* characteristics with prominent edge effect

Shown in Figure 6.12 is an actual data obtained using the miniaturized shielded Gerdien condenser for bias voltage of 0 to 50 V. A droop in the measured current has been observed in the *I-V* characteristics when the applied voltage exceeds the saturation voltage which is at around 10 V. Although the region after the saturation in the *I-V* characteristics is not needed for the calculation of ion mobility and density, this occurrence is discussed in this section.

The electric field inside the Gerdien condenser is studied through computer simulation called *HiPhi* solution in the *Field Precision LLC* program. The parts of each region is shown in Figure 6.13 and their respective settings are shown in Table 6.6. Note that in this simulation, the y-axis corresponds to the axis parallel to the air flow.

Table 6.6 Simulation settings for each regions

Inner (V)	Outer (V)	Insulator (ε)	Shield (V)	Solution volume (ε)
0	10	3.7	0	1.0

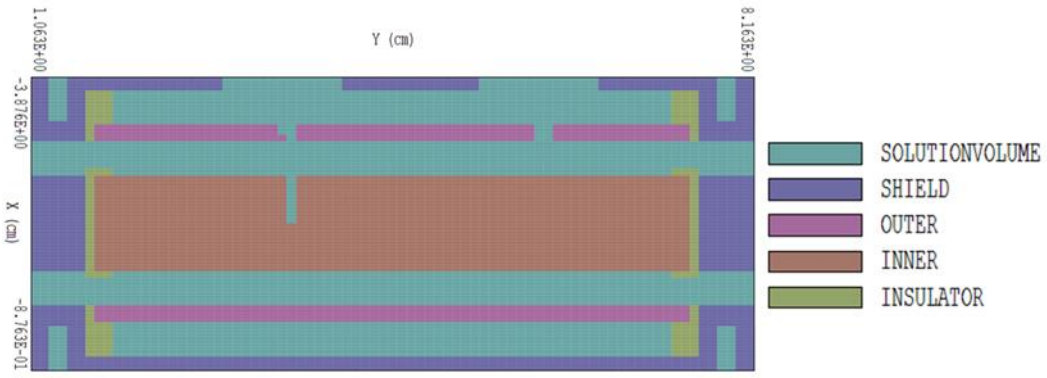

Figure 6.13 Parts of each regions for edge effect simulation

6.5.2 Results

Figure 6.14 shows the electric field simulation demonstrating the concentration of electric field on the region near the ends of the outer electrode. It is assumed that when the applied voltage is much higher than the saturation voltage, the amount of deflected ions increases due to more pronounced edge effect.

In order to calculate for the effective area of the Gerdien condenser conduit, the electric field distribution from the edge of the inner electrode to the outer electrode's edge is plotted as shown in Figure 6.15.

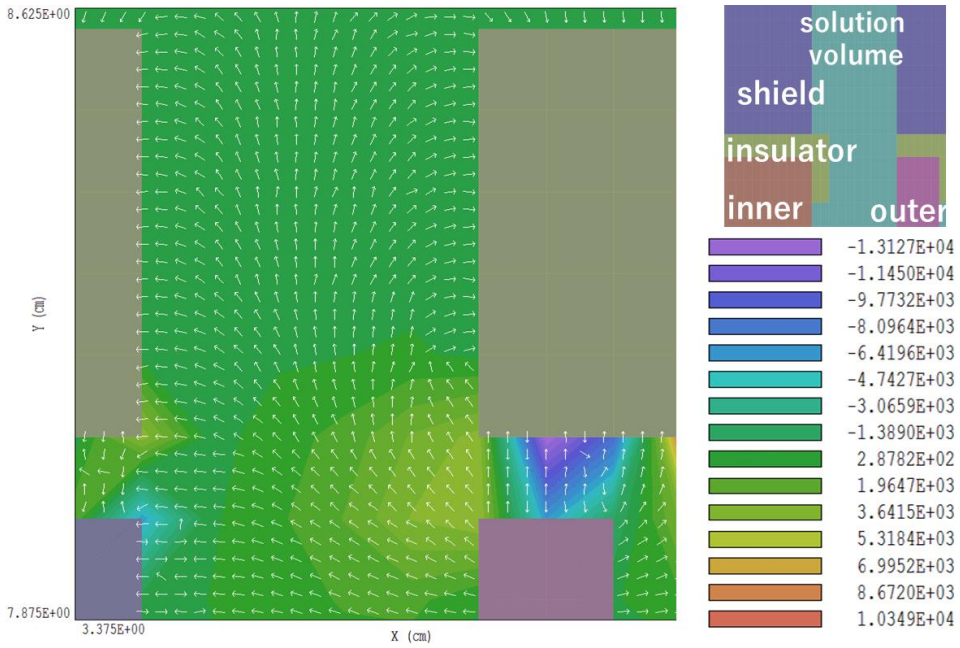

Figure 6.14 Electric field simulation demonstrating edge effect

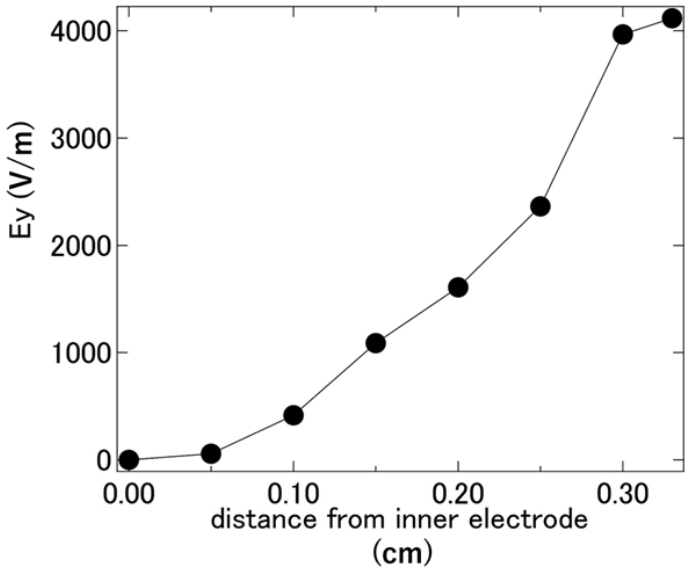

Figure 6.15 Electric field distribution along the radial axis at the end of the electrodes

The inhomogeneity in electric field distribution along the y-axis is evident from Figure 6.15. The effective area of the Gerdien condenser for collecting ions can be determined if the critical electric field is known. It is expected that when the applied voltage is increased over the saturation voltage, the effective area becomes smaller wherein some of the electric field along y-axis exceeds the value of the critical electric field thereby deflecting ions away from the collector electrode. This in turn results to decrease in measured current as observed in the *I-V* characteristics.

In order to solve for the effective area of the Gerdien condenser, the critical electric field, E_c should be calculated, given by the equation:

$$E_c = \frac{v_f}{\mu_c} \tag{6.1}$$

where, v_f is the velocity of ions along the y - axis which is determined by the fan velocity, and μ_c is the mobility of the slowest ion that is sought to be collected. When the value of E_c is known, the corresponding effective radius, r_c, can be determined through the electric field simulation.

Supposed that the fan flow rate of 750 cm^3/s is used, if the ion of lowest mobility is sought to be collected, then,

$$E_c = \frac{750}{\pi(0.85^2 - 0.5^2) \times 1.5} \tag{6.2}$$

$$\cong 337 \frac{\text{V}}{\text{cm}} \text{ or } 3.37 \times 10^4 \frac{\text{V}}{\text{m}}$$

The calculated value of critical electric field is too large if compared to the simulated electric field inside the Gerdien condenser. Hence, the air velocity is also confirmed through computer simulation.

Figure 6.16 shows the air velocity simulation along the y - axis done through *Autodesk CFD.* There is an evident drop in air velocity inside the Gerdien condenser's

conduit due to the pressure gradient. Although there is an observed decrease in the velocity inside the Gerdien condenser, the resulting order of magnitude of the critical electric field remains the same.

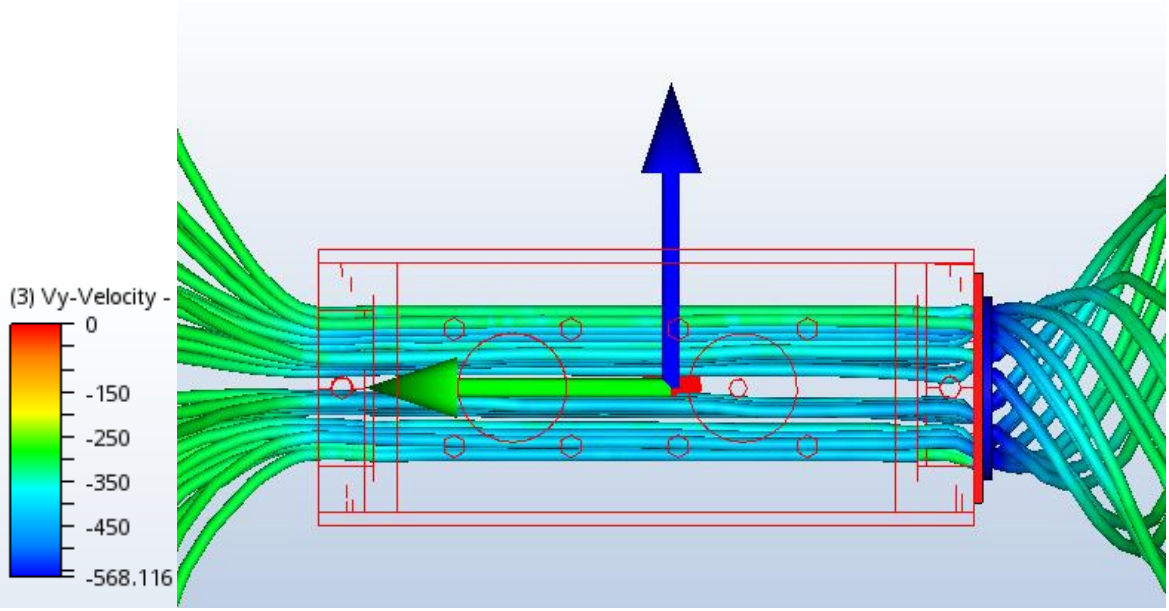

Figure 6.16 Air flow simulation inside the Gerdien condenser conduit

Although there is inhomogenous electric field distribution at the ends of the condenser due to the edge effect, it is not adequate to cause the droop observed in the current-voltage characteristics even when the reduction in air velocity is accounted. More detailed analysis on the effect of space charge as well as the resulting neutral-ion recombination due to charge accumulation in the conduit of the Gerdien condenser should be considered for future work.

6.6 Summary

The flow rate of the fan attached to the Gerdien condenser is characterized in order to confirm the calculation of ion density and mobility from the obtained current-voltage characteristics. The effect of the fan flow to the measurements has also been investigated for a fixed Gerdien condenser to ion source distance of 2.0 cm. The change in air flow rate on the Gerdien condenser is observed to influence the calculated ion density significantly: an increase in fan flow rate yielded to a decrease in ion density due to enhanced ion recombination.

The effect of electrode material to the Gerdien condenser *I-V* characteristics are studied to investigate suitable material for atmospheric pressure plasma diagnostics. The *I-V* characteristics yielded different electrode potential dependent on the material and its surface condition. There were observed shifts in the ion mobility spectra, but the ion species detected by the condenser remain nearly unaltered if the electrode potential shift is considered. The calculated ion density differs depending on the material, but the deviations were less than an order of magnitude difference.

Electric field simulation is done to observe the fringing field at the edge of the Gerdien condenser. Through the results of simulations, it is confirmed that the edge effect is not the predominant reason on the observed droop in the curent-voltage characteristics. However, further investigation is still needed in order to confirm the air velocity inside the conduit in simultaneous with the possible contribution of space charge and ion recombination inside the Gerdien condenser.

Chapter 7
Conclusions

This dissertation demonstrates the diagnostics of laboratory-produced atmospheric pressure plasmas based on the Gerdien condenser diagnostic technique. The instrument is designed and fabricated to match the plasma plume dimension produced at atmospheric pressure. The Gerdien condenser is shown to be capable of identifying the ion species and ion densities present in dense and dilute plasma plumes produced by a 13.56 MHz RF power source. After the proof of principle, the instrument design and geometry was improved further to make the acquired data quality more reliable. The factors that influences the measured current-voltage characteristics are analyzed individually from a component to another; the ion distribution along the ion production region is investigated as well as the effect due to flow rate into the current measurement; the effect of surface work function and surface condition are also studied; the edge effect to the current-voltage characteristics is also explored. The detailed summary of the results are discussed in the remainder of this chapter. Future prospects on further development of the new technique are also presented.

7.1 On plasma excitation

Atmospheric pressure plasmas are successfully produced on systems with capacitively coupled configuration and needle-shaped electrode setup using a 13.56

MHz radio frequency power source. With the capacitively coupled configuration, dilute plasma plumes are produced even at higher input forward powers and low measured reflected power. Longer plume dimensions are sustained when swirl gas is introduced into the system. On the other hand, denser plume discharge and better impedance matching is attained when the needle-shaped electrode device is employed. In addition, there is no need for swirl gas employment for the needle-shaped electrode configuration. However, the maximum input power is limited due to the damage observed in the tungsten rod which acts as the discharge tip of the needle-shaped electrode. Also, arcing occurs on the plasma exit nozzle between the electrodes where filamentary structures are observed when the input power is too large. Optical emission spectroscopy shows the presence of Ar, N_2 and O_2 species on the produced plume with density assumed to be proportional to input parameters based on the plasma glow image analysis.

7.2 On pointed inner electrode Gerdien condenser

The miniaturized Gerdien condenser measurement with design based on rocket-borne air ion measurements proves that the principle of Gerdien condenser is successfully adapted for laboratory-produced atmospheric pressure plasma application. Positive ion mobility, hence positive ion species and their corresponding densities are measured by the adapted technique with reasonable stability. The device is also tested for measuring the ion density distribution on the axis along the ion source production. However, the apparent contribution of noise to the current measured is evident especially when the distance of the Gerdien condenser from the ion source is

large. Therefore, improvement on the pointed inner electrode Gerdien condenser instrument was necessary.

7.3 On shielded Gerdien condenser

The improved design of the miniaturized Gerdien condenser shows significant noise reduction in the acquired signal. The current-voltage characteristics produced by the shielded Gerdien condenser is therefore concluded to be more reliable for data analysis than the pointed inner electrode Gerdien condenser.

Two kinds of laboratory-produced atmospheric pressure plasmas are characterized with the shielded Gerdien condenser, particularly dense and dilute plasma plume. Similar to the pointed inner electrode Gerdien condenser, the diffusion of charged particles into the flow conduit is detected when the bias voltage is equal to zero resulting into a current offset. However in this case, the observed offset is more evident when the flow rate from the ion source is higher such as for the case when the swirl gas is included.

The detected ion species for both ion sources are O^+, O_2^+, Ar^+ and N_2^+ which are the same with the one acquired by the previous version of the Gerdien condenser. The difference in the intensities of the dense and dilute plasma plume that is observable through image analysis and optical emissions spectroscopy is quantified by measuring the ion density as acquired by the Gerdien condenser measurement. The Gerdien condenser is also successful in detecting negative ions when voltage of opposite polarity is applied into the bias electrode.

7.4 On the individual components of the Gerdien condenser

The components of the Gerdien condenser which is mainly comprised of the electrodes and the fan are characterized individually in order to isolate their effect to the measured current-voltage characteristics. It has been observed that the increase in fan velocity greatly contributes to the decrease in detected ion density while there is no apparent effect on the attained ion mobility.

The current-voltage characteristics is also dependent on the surface condition of the material. The surface work function which is dependent on the surface condition and the type of material affects the produced electric field for a given bias potential difference and consequently the shift in ion mobility. However, the ion species detected by the condenser remain nearly unaltered if the electrode potential shift is considered. The calculated ion density differs depending on the material, but the deviations were less than an order of magnitude.

Electric field simulation is done to observe the effect of fringing field at the edge of the Gerdien condenser. Results shows that the calculated critical electric field is too large compared to the magnitude of electric field on the edge of the electrodes. Hence, the edge effect is not the predominant factor on the decrease in measured current after saturation current is attained. However, further investigation is still needed to confirm the air velocity inside the conduit simultaneously with the possible contribution of space charge and the resulting neutral- ion recombination inside the Gerdien condenser.

7.5 Further work

The ion mobilities in this study are compared from the experimental data of mass-identified ions in neutral gas at room temperature. Hence, there is a need to establish an ion mobility spectra of higher resolution based on measurements acquired from laboratory-produced atmospheric pressure plasmas. The shifts in ion mobilities depending upon the work function of the material used as electrode has to be considered.

The air velocity profile inside the conduit has to be carefully reanalyzed in order to understand the descend of ion current at larger bias voltage in the current-voltage characteristics of the Gerdien condenser. The effects of space charge as well as the positive ion and negative ion mutual recombination to the current measurement should be analyzed in order to improve the accuracy of the data. Further work is also sought for the improvement on the instrumentation. In order to develop a probe-like Gerdien condenser, the effect of the instrument dimension should be considered and the signal handling electronics should be improved.

References

Aplin, K. L. *Instrumentation for atmospheric ion measurements* (2000). PhD Thesis. University of Reading. August (2000)

Baglin V., Bojko J., Grobner O., Henrist B…. Taborelli M., "The secondary electron yield of technical materials and its variation with surface treatments". Proceedings of EPAC, Vienna Austria (2000).

Bogaerts, A., Neyts, E., Gijbels, R., & Van der Mullen, J. "Gas discharge plasmas and their applications". *Spectrochim. Acta - Part B At. Spectrosc.*, **57**, 4, 609–658 (2002).

Brownlee J. N. "A fast mobility spectrometer for atmospheric ions". PhD Thesis, University of Auckland (1973).

Burt, D. A. *Development of a Gerdien condenser for sounding rockets*. Bedford, Massachusetts (1967).

Cada, M., Hubicka, Z., Sicha, M., … Tichy, M. "Probe diagnostics of the RF barrier-torch discharge at atmospheric pressure". *Surf. Coatings Technol.*, **174–175**, 530–534 (2003).

Chabert, P., & Braithwaite, N. *Physics of Radio-Frequency Plasmas*. *Cambridge University Press, New York* (2011).

Chalmers, J. A.. Atmospheric Electricity, Pergamon Press, Oxford, UK (1967). Material from the source not available but quoted in secondary source (Flagan 1998).

Conrads H., Schmidt M.. "Plasma generation and plasma sources". Plasma Sources Sci. Technol. 9 441–454 (2000).

Coulomb, C. A.. Mem. Acad. Sci. Paris, 616 (1795). Material from the source not available but quoted in secondary source (Flagan 1998).

Croskey C., Mitchell J.D., Friedrich M. "Investigation of atmospheric neutral constituent by photoionziation technique". Proceedings of the 16th ESA Symposium on European Rocket and Balloon Programmes and Related Research, (2003).

Das, M. "Studies on Atmospheric Electric Parameters", , March (1993).

Ellis, H. W., Thackston, M. G., McDaniel, E. W., & Mason, E. A. "Transport Properties of gaseous ions over a wide energy range Part III". *At. Data Nucl. Data Tables*, **31**, 1, 113–151 (1984).

Fanara, C., & Richardson, I. "A Langmuir multi-probe system for the characterization of atmospheric pressure arc plasmas". *J. Phys. D. Appl. Phys.*, **34**, 2715–2725 (2001).

Flagan, R. C. "History of Electrical Aerosol Measurements". *Aerosol Sci. Technol.*, **28**, February 2015, 301–380 (1998).

Fridman, G., Brooks, A. D., Balasubramanian, M., … Friedman, G. "Comparison of direct and indirect effects of non-thermal atmospheric-pressure plasma on bacteria". *Plasma Process. Polym.*, **4**, 4, 370–375 (2007).

Hatakeyama H., Kobayashi J., Kitaoka T., Uchikawa K. "A radiosonde instrument for the measurement of atmospheric electricity and its flight results" in Smith L.G. "Recent advances in atmospheric electricity" Pergamon Press, Oxford (1958).

Harrison, R. G., & Aplin, K. L. "Multimode electrometer for atmospheric ion measurements". *Rev. Sci. Instrum.*, **71**, 12, 4683 (2000).

Higazi, K. A., & Chalmers, J. A. "Measurements of atmospheric electrical conductivity near the ground". *J. Atmos. Terr. Phys.*, **28**, 327–330 (1966).

Israel, H.. "Atmospheric Electricity. vol. I: Fundamentals, Conductivity, Ions". Israel Program for Scientific Translations, Jerusalem (1970). Material from the source not available but quoted in secondary source (Flagan 1998).

Iza, F., Kim, G. J., Lee, S. M., … Kong, M. G. "Microplasmas: Sources, Particle Kinetics, and Biomedical Applications". *Plasma Process. Polym.*, **5**, 4, 322–344 (2008).

Kabouzi, Y., Calzada, M. D., Moisan, M., … Trassy, C. "Radial contraction of microwave-sustained plasma columns at atmospheric pressure". *J. Appl. Phys.*, **91**, 3, 1008–1019 (2002).

Kelvin, L. "On the Necessity for Incessant Recording, and for Simultaneous Observations in Different Locations to Investigate Atmospheric Electricity". Macmillan, London, 227-229 (1859). Material from the source not available but quoted in secondary source (Flagan 1998).

Kolpaková, A., Kudrna, P., & Tichý, M. "Study of Plasma System by OES (Optical Emission Spectroscopy)". In *WDS'11 Proceedings of Contributed Papers* (pp. 180–185) (2011).

Kong, M. G., Kroesen, G., Morfill, G., … Zimmermann, J. L. "Plasma medicine: An introductory review". *New J. Phys.*, **11** (2009).

Machala, Z., Janda, M., Hensel, K., … Morvová, M. "Emission spectroscopy of atmospheric pressure plasmas for bio-medical and environmental applications". *J. Mol. Spectrosc.*, **243**, 2, 194–201 (2007).

McDaniel E. W., and Mason E. "The mobility and diffusion of ions in gases". Wiley 1973.

Merche, D., Vandencasteele, N., & Reniers, F. "Atmospheric plasmas for thin fi lm deposition : A critical review". *Thin Solid Films*, **520**, 13, 4219–4236 (2012).

Mullen, J. ., Madson, J., Medgyesi-Mitschang, L. ., … Doane, P. . "Diagnostic techniques for high temperature plasma reactions". *Chem. Eng. Progr., Symp*, **112**, 74–84 (1971).

Ohtsu, Y., & Tanaka, S. "Production of Capacitively Coupled Atmospheric Plasma Jet With Multiring Electrodes for the Medical Plasma Tool". *IEEE Trans. Plasma Sci.*, **37**, 11, 2221–2227 (2009).

Pedersen, A. "Measurements of ion concentrations in the D-region of the ionosphere with a Gerdien condenser rocket probe". *Tellus XVIII*, **1** (1965).

Porteanu, H. E., Kühn, S., & Gesche, R. "Electric probe investigations of microwave generated, atmospheric pressure, plasma jets". *J. Appl. Phys.*, **108**, 1, 13301 (2010).

Rose, G., & Widdel, H. U. "Results of Concentration and Mobility Measurements for Positively and Negatively Charged Particles Taken Between 85 and 22 km in Sounding Rocket Experiments", **7**, 1, 81–87 (1972).

Rutherford, E. "The Velocity and Ratc of Recombination of the Ions in Gases Exposed to Rongten Radiation" Phil. Mag. **44**, 422-440 (1897). Material from the source not available but quoted in secondary source (Flagan 1998).

Schott, L. "Electrical Probes" in W. Lochte-Holtgreven. "Plasma Diagnostics" North-Holland Publishing Co. Amsterdam, **11**, 668-731 (1968).

Smith, D. K. *Investigation of the performance of a gerdien condenser in low density supersonic flow*. Tennessee (1968).

Tammet, H. "The Aspiration Method for the Determination of Atmospheric-Ion Spectra". Israel Program for Scientific Translations, Jerusalem, (1970).

Tendero, C., Tixier, C., Tristant, P., … Leprince, P. "Atmospheric pressure plasmas: A review". *Spectrochim. Acta Part B At. Spectrosc.*, **61**, 1, 2–30 (2006).

Viehland, L. A., & Mason, E. A. "Transport Properties of Gaseous Ions Over a Wide Energy Range, IV". *At. Data Nucl. Data Tables*, **60**, 1, 37–95 (1995).

Volta, A. “Dcl modo di render sensibilissima la piu debole electriciti si naturale sia artivicalc”. Phil. Trans. Roy. Soc. 72, 237-280(1782). Material from the source not available but quoted in secondary source (Flagan 1998).

Wahlin, L. *Atmospheric Electrostatics*. Letchworth, Hertfordshire, England: Research Studies Press (1989).

Widdel, H. U., Rose, G., & Borchers, R. "Experimental results on the variation of electric conductivity and ion mobility in the mesosphere". *J. Geophys. Res.*, **81**, 34, 6217–6220 (1976).